Rain Production in Convective Clouds As Simulated in an Axisymmetric Model with Detailed Microphysics. Part I: Description of the Model

TAMIR REISIN, ZEV LEVIN, AND SHALVA TZIVION

Department of Geophysics and Planetary Sciences, Raymond and Beverly Sackler Faculty of Exact Sciences, Tel Aviv University, Ramat Aviv, Israel

(Manuscript received 10 February 1995, in final form 21 August 1995)

ABSTRACT

A hydrodynamic nonhydrostatic anelastic numerical model of an axisymmetric convective cloud is described in which the microphysical processes are treated in detail for different species of hydrometeors: drops, ice crystals, graupel, and snow particles. The size distribution function for each type of particle is divided into 34 spectral bins. In each spectral category two physical moments of the distribution function (number and mass concentration) are independently calculated using the method of moments. The following physical processes are computed: nucleation of drops and ice crystals, freezing of drops, diffusional growth/evaporation of drops and ice particles, collisional coalescence of drops and ice particles, binary breakup of drops, melting of ice particles, and sedimentation. The model describes the different stages of cloud development, the formation of ice, its growth by deposition and riming, the formation of graupel, and the precipitation stage. Analysis of the distribution functions for the different species provides insight into the different microphysical processes active in rain formation in mixed clouds. As an illustration of the capability of the model, the simulation of a mixed-phase continental cloud is presented.

1. Introduction

Numerical models of clouds are useful tools for studying the complex processes of rain formation. While models with parameterized schemes of microphysical processes can efficiently simulate the dynamic fields and other general properties of the clouds, the study of rain formation and its sensitivity to changes in cloud condensation nuclei (CCN) and ice nuclei (IN) spectra requires a detailed treatment of the microphysical processes.

The microphysical processes in warm clouds are fairly well understood, and several models are available that simulate the growth of such clouds (e.g., Tzivion et al. 1994; Kogan 1991). Models of cold clouds must handle the more complex microphysics of the ice phase. These complexities stem from the large number of stochastic equations that require simultaneous solution, the mathematical problems involved in obtaining these solutions, and the scarcity of experimental data on a large number of parameters related to physical processes involving ice particles in clouds. For example, collision efficiencies are known only for a very limited range of particle sizes and shapes. It is not surprising, therefore, that there are only a few models with explicit ice microphysics: Cotton (1972) (Lagrangian model), Danielsen et al. (1972), Scott and Hobbs (1977), Nelson (1979), and Tzur and Levin (1981), which includes electrification processes (1.5D); the 2D model by Young (1974a,b), with prescribed dynamics; Takahashi (1976), axisymmetric; Hall (1980), 2D; Khvorostyanov et al. (1989), 2D; and Alheit et al. (1990), 1D (which includes chemical processes).

The last four publications are the most up to date and relevant to the model described here. Takahashi's axisymmetric model of a hailstorm cloud (1976) includes a large number of microphysical processes as well as an interesting scheme for treating the changing shapes of the ice crystals, but their mathematical formulation is highly simplistic in light of present knowledge.

Hall's model (1980) concerns primarily the formation of graupel particles by riming of platelike ice particles that originated from activated IN and grow by diffusion of water vapor. The ice spectrum is assumed to be represented by a single distribution function where the ice particle type and bulk density are prescribed functions of particle category. The ice particle spectrum is divided into three regions: the first region (50–400 μm) corresponds to ice crystals with bulk density of 0.4 g cm^{-3}; the second region (400–600 μm) is a transition region with linearly increasing bulk density; and the third region (600–8410 μm, bulk density of 0.8 g cm^{-3}) is for graupels. This classification and the density distribution differ significantly from the

Corresponding author address: Dr. Zev Levin, Department of Geophysics and Planetary Science, Raymond and Beverly Sackler Faculty of Exact Sciences, Tel Aviv University, 69978 Ramat Aviv, Israel.
E-mail: zev@hail.tau.ac.il.

approach adopted here, as will be explained later. The ice phase processes presented in Hall focus on graupel formation from ice crystals produced by nucleation; they ignore the creation of snowflakes by aggregation or the presence of relatively large ice crystals that do not become graupel. Further drawbacks of Hall's model are the inability to produce small graupel, the lack of consideration given to drops freezing, and the fact that the collisions between ice particles and drops are not treated as a stochastic process.

Khvorostyanov et al.'s model (1987, 1989) includes distribution functions for water drops and ice particles. It was used for numerical simulations of seeding, but while the supersaturation field is relatively well treated, the nonstochastic treatment of the microphysical processes could lead to unrealistic results.

The model of Alheit et al. (1990) can be considered an improvement or refinement of Hall's model, in 1D, and is based on Flossmann et al.'s model (1985) for warm clouds. Here, the distribution function of ice particles and graupel are considered separately. Even though the interactions between all the species are considered in more detail, their formulation is not fully stochastic. Parameters of the ice shape are included, and the diffusional growth scheme is refined. Snow formation (aggregates of ice) and the melting process are not considered in the model. Great effort was made to treat the interactions with aerosols, both inside the particles and interstitial.

The present work describes an axisymmetrical nonhydrostatic anelastic model of a convective cloud with a detailed treatment of the microphysical processes. This model is based on the warm cloud model presented in Tzivion et al. (1994) modified to include ice processes. The added microphysical processes are nucleation of IN, drop freezing, diffusional growth (and evaporation) in a mixed-phase environment, ice–ice and drop–ice coagulation, and melting and sedimentation of ice particles. Three types of ice particles are considered: ice crystals, graupel, and snow particles. Equations are formulated and solved for all the microphysical processes included. The numerical method used in the mathematical treatment of these processes is the method of multimoments, developed at Tel Aviv University (Tzivion et al. 1987, 1989; Feingold et al. 1988). This method provides the accuracy required for the numerical study of rain formation processes.

The wide scope of this work necessitated dividing it into two parts. This paper describes the numerical model and presents the results for one type of continental cloud.

2. The cloud model

The axisymmetrical nonhydrostatic model of a convective cloud with detailed microphysics is an updated version of the one put forth by Tzivion et al. (1994, hereafter TRL) modified to include cold processes. The dynamic components are described briefly [for a full description see Tzivion et al. (1984), Reisin et al. (1988), Feingold et al. (1991), and TRL], while the microphysical processes are covered in detail.

a. The dynamic model

The system of equations describing the formation and evolution of an axisymmetric nonhydrostatic anelastic convective cloud over a homogeneous boundary surface is basically the same as presented in TRL. We solved equations of motions for the vertical and radial velocity (w and u, respectively), equations for the virtual potential temperature perturbation (θ_v) and the specific vapor perturbation (q), and a diagnostic equation for the pressure perturbation. The equations for specific mass and number of drops were modified to include processes that involve ice, like freezing and melting. Equations for the specific mass and number of the different ice species were added, and since the nucleation of drops was modified, a new equation for the CCN particles was formulated. Definitions of all symbols can be found in appendix A.

The equations for the different substances in the model are as follows:

$$\frac{\partial M_{w_k}}{\partial t} = F_q(M_{w_k}) - D(M_{w_k}) + \left(\frac{\delta M_{w_k}}{\delta t}\right)_{\text{nucl}} + \left(\frac{\delta M_{w_k}}{\partial t}\right)_{\text{cond/evap}} + \left(\frac{\delta M_{w_k}}{\partial t}\right)_{\text{coll/breakup}} + \left(\frac{\delta M_{x_k}}{\delta t}\right)_{\text{melting}} - \left(\frac{\delta M_{w_k}}{\delta t}\right)_{\text{freezing}} + \left(\frac{\delta M_{w_k}}{\delta t}\right)_{\text{sedim}} \quad (1)$$

$$\frac{\partial M_{x_k}}{\partial t} = F_q(M_{x_k}) - D(M_{x_k}) + \delta_{xi}\left(\frac{\delta M_{i_k}}{\delta t}\right)_{\text{nucl}} + \left(\frac{\delta M_{x_k}}{\delta t}\right)_{\text{depos/sublim}} + \left(\frac{\delta M_{x_k}}{\delta t}\right)_{\text{coll}} - \left(\frac{\delta M_{x_k}}{\delta t}\right)_{\text{melting}} + (1 - \delta_{xs}) \times \left(\frac{\delta M_{w_k}}{\delta t}\right)_{\text{freezing}} + \left(\frac{\delta M_{x_k}}{\delta t}\right)_{\text{sedim}} \quad (2)$$

$$\frac{\partial N_{\text{CCN}_k}}{\partial t} = F_q(N_{\text{CCN}_k}) - D(N_{\text{CCN}_k}) - \sum_{k=1}^{J_{\text{CCN}}} \left(\frac{\delta N_{\text{CCN}_k}}{\delta t}\right) \quad (3)$$

$$\frac{\partial N_{\text{act ice}}}{\partial t} = F_q(N_{\text{act ice}}) - D(N_{\text{act ice}}) + \sum_{k=1}^{J} \left(\frac{\delta N_{i_k}}{\partial t}\right). \quad (4)$$

The dynamic equations for the category mass concentration M_{w_k} for water are shown in Eq. (1) and for ice particles in Eq. (2). Here, x represents the species of ice particles in the model: ice crystals (i), graupel (g), or snow particles (s) (described later). The terms appearing at the end of Eqs. (1) and (2) denote the contributions of the microphysical processes. The Kroenecker delta in Eq. (2) is used for selecting the species that participate in the process. Similar equations are formulated for the category number concentration of the water and ice species (N_{w_k} and N_{x_k}, respectively). Equation (3) represents the concentration of available CCN particles in category k. The last term is for the number of newly activated CCN particles as determined by the nucleation process. Equation (4) is for the concentration of activated ice particles by nucleation on IN.

In the above equations, $D(\phi)$ and $F_q(\phi)$ are the advective and turbulent diffusion operators as defined in TRL. For the turbulence coefficient we used a semiempiric approach based on Monin and Yaglom (1967).

Computation time was reduced by using movable side and upper boundaries as follows:

$$R(t) = L_r \left(\frac{t}{t_{ch}}\right)^{\alpha}$$

and

$$H(t) = H_t \left(\frac{t}{t_{ch}}\right)^{\alpha}, \tag{5}$$

where $R(t)$ is the lateral boundary, L_r is the size of the domain in the radial direction (6000 m in this work), $H(t)$ is the upper boundary, and H_z is the size of the domain in the vertical direction (9000 m in this study). The parameter t_{ch} is the characteristic time of the simulation (about 1 h), and α is a constant parameter that depends on the rate of convective development (usually around 0.2), such that the results are the same as those obtained with fixed boundaries.

All equations were solved using an explicit forward time difference scheme. Spatial derivatives were formulated in conservative form using a second-order scheme according to Bryan (1966), which avoids nonlinear instabilities. For positive-definite variables like number and mass concentrations, a first- or second-order positive-definite hybrid scheme was used, similar to that of Hall (1980). The numerical procedures and the coupling of the microphysics and dynamics are similar to Ogura and Takahashi (1973) and Soong (1974).

In all simulations the grid size was set to 150 m in the radial direction and 300 m in the vertical, and the dynamic time step was 5 s. Open boundaries conditions were assumed for all the variables.

b. *The microphysical model*

The temporal changes in the particles size distribution function $n(m, z, r, t)$ with respect to mass m at location (z, r) and time t due to microphysical processes can be written as

$$\frac{\partial n_y(m, z, r, t)}{\partial t} = \left[\frac{\delta n_y(m, z, r, t)}{\partial t}\right]_{\text{nucl}} + \left[\frac{\delta n_y(m, z, r, t)}{\partial t}\right]_{\text{cond/evap, depos/sublim}} + \left[\frac{\delta n_y(m, z, r, t)}{\partial t}\right]_{\text{coll/breakup, ice interac}} + \left[\frac{\delta n_y(m, z, r, t)}{\delta t}\right]_{\text{sedim}} + \left[\frac{\delta n_y(m, z, r, t)}{\partial t}\right]_{\text{freezing}} + \left[\frac{\delta n_y(m, z, r, t)}{\delta t}\right]_{\text{melting}}, \tag{6}$$

where $n_y(m, z, r, t)$ is the size distribution function of the species y: water drops, ice crystals, graupel, or snow particles.

Figure 1 is a schematic representation of the different microphysical processes considered in the model.

Ice crystals were created by nucleation of IN or by freezing of drops smaller than 100 μm in radius. We assumed that ice crystals are mostly nucleated in the temperature range $-10°$ to $-20°$C, where planar-type crystals are formed (Alheit et al. 1990). The ice crystals were assumed to be oblate spheroids. Snow particles formed by aggregation of ice crystals and were considered to be spherical. Graupel particles were spherical and were formed by freezing of drops with radii larger than 100 μm and/or by different processes of particles coagulation, as will be explained later. The density of the graupel was assumed to be 0.4 g cm^{-3}; hail formation was not considered. The ice crystal density varied from 0.9 g cm^{-3} for the smallest particles down to 0.45 g cm^{-3} for the biggest. The density for the snow particles was fixed at 0.2 g cm^{-3}.

The particles spectrum was divided into 34 bins (x_k, $k = 1, \cdots, 34$), with mass doubling in each bin:

$$x_{k+1} = 2x_k. \tag{7}$$

The initial mass was $x_1 = 1.598 \times 10^{-11}$ g, corresponding to drops with a diameter of 3.125 μm. The maximum mass was $x_{35} = 1.7468 \times 10^{-1}$ g, which corresponds to drops 8063 μm in diameter.

The multimoments method was used in all mathematical formulations. This method, based on Tzivion (1980) and Tzivion et al. (1987), solves for two or more physical moments of the particle distribution function while maintaining the balance between the different moments. To obtain a set of moment equations for each bin for each species, the operator $\int_{x_k}^{x_{k+1}} m^j dm$ is applied to both sides of Eq. (6). In the present case we solve for the two first moments of the category distribution function, N_{y_k} and M_{y_k}, the number and mass concentration of species y in the kth bin, respectively:

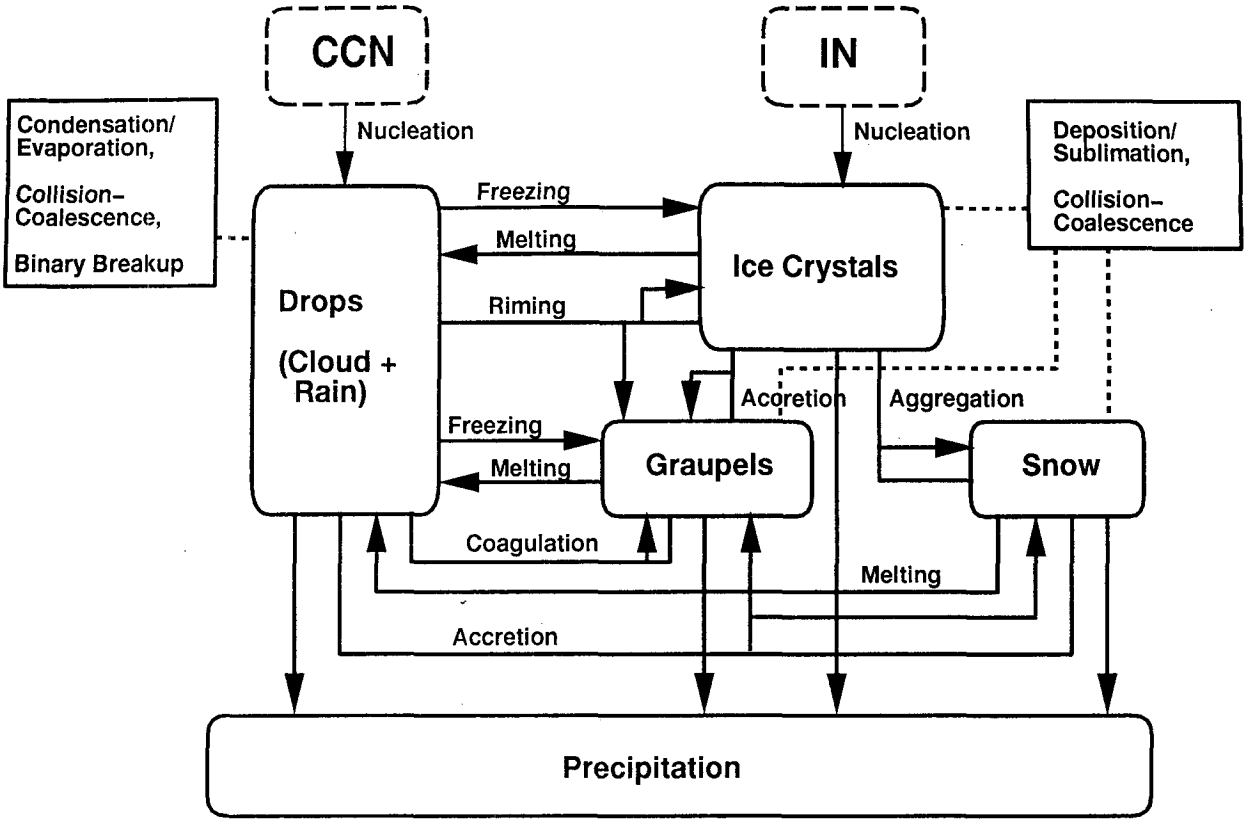

FIG. 1. Schematic representation of the microphysical processes considered in the model. The dashed lines indicate processes that include only interactions with particles of the same kind. Solid lines connect interacting species, and arrows point in the direction of the result.

$$N_{y_k} = \int_{x_k}^{x_{k+1}} n_{y_k}(m, t)dm, \tag{8}$$

$$M_{y_k} = \int_{x_k}^{x_{k+1}} m n_{y_k}(m, t)dm. \tag{9}$$

Here, y represents drops (w), ice crystals (i), graupel (g), or snow (s) particles. The dependence on z and r is implicit in the above equations. As Tzivion et al. (1987) showed, the category distribution function n_{y_k} is prescribed only when the integration is over an incomplete category interval. In such cases the distribution function is approximated using a linear function, positive within the category. A nondimensional parameter that relates different moments is used to close the system of the category moment equations. The two-moment approach gives a relatively accurate and efficient method to solve equations of microphysical processes in clouds. In comparison to one-moment numerical methods (e.g., Bleck 1970), the average mass in a category ($\bar{m}_k = M_k/N_k$) is not constrained to remain constant but can change in time according to the number and mass concentration in the category.

The time step for all the microphysical processes, apart from diffusional growth or evaporation processes, was 5 s.

1) NUCLEATION OF WATER DROPS

The number of drops that can be activated at a certain supersaturation is determined according to a CCN activation spectra in the form (Twomey 1959)

$$\bar{N}_{\text{act}} = N_0 S_w^{\alpha}, \tag{10}$$

where $\bar{N}_{\text{act}}$ is the number concentration of drops that can be activated at a certain supersaturation $S_w(\%)$ (with respect to water) and N_0 and α are empirical parameters (different for continental and maritime clouds).

To account for the fact that CCN of different sizes are activated at different supersaturations, we divided the number concentration of the CCN particles into six discrete categories as a function of the critical supersaturation according to

$$N_{\text{CCN}_k} = N_{0_k} \mathcal{F}_k(S_{w_k}), \quad k = 1, \cdots, 6, \tag{11}$$

where $\mathcal{F}_k(S_{w_k})$ is some function of the supersaturation. For supersaturations lower than 1%, this function was equal to the usual S_w^{α}, as in Eq. (10). CCN activation spectra are usually measured for supersaturations lower than 1%, extrapolating these spectra to higher supersaturation might produce very high concentrations of

activated drops. Therefore, in order to constrain the increase of N_{CCN_k} with the supersaturation, we assumed that for high supersaturations $\mathcal{F}_k = \exp[(S_{w_k} - 1)/10]$. In this approach we were inspired by Flossmann (1991), who showed that the number of CCN active at a certain supersaturation increases very little for supersaturations higher than 1%. At each time step, $\bar{N}_{act}$ is calculated according to Eq. (10) and compared with the available CCN spectra N_{CCN_k}. The number of new drops activated is given by the minimum between $(\sum_1^{k,S_{w_k}<S_w} N_{CCN_k})$ and $\bar{N}_{act}$.

Finally, the CCN spectrum is updated based on the number of drops actually nucleated. CCN are depleted according to their activation efficiency: the most efficient ones, those that nucleate first, get depleted first. In the next time step the dynamic Eq. (3) is applied.

Newborn drops are distributed according to a predetermined function. We considered two such functions: a complete gamma function and an exponential function. The distribution in the former is in the form

$$f(r) = Ar^{\beta}e^{-Br^{\gamma}}, \tag{12}$$

where β and γ are parameters. Parameters A and B are functions of β, γ, and $\bar{r}$ (the average radius of the nucleated drops distribution), and the normalization is carried out according to the number of nucleated drops. For maritime clouds we used $\beta = 2$, $\gamma = 1$, and $\bar{r} = 11$ μm (a broad spectrum) and for moderate maritime clouds $\beta = 6$, $\gamma = 4$, and $\bar{r} = 5$ μm (a narrower spectrum).

Even when using the parameters for narrow spectra, the drop spectrum produced by the complete gamma function has a long tail containing a few large drops. Such a spectrum is inappropriate for simulating extreme continental clouds. In those cases we used an exponential function in the form

$$f(r) = Ae^{-r/\bar{r}}, \tag{13}$$

where $\bar{r}$ is the average radius of the distribution. The coefficient A is found by normalization of $f(r)$. For both functions we assumed the average mass of the nucleated drops to be $1.5x_k$.

In cases where the complete gamma function was used, the average radius of the distribution was considered to be a function of the supersaturation—the higher the supersaturation, the smaller the average radius—according to

$$\bar{r} = \bar{r}_{max}\exp(-S_w/\bar{S}). \tag{14}$$

For maritime clouds we used $\bar{r}_{max} = 11$ μm and $\bar{S} = 7.2$ and for the continental clouds $\bar{r}_{max} = 5$ μm and $\bar{S} = 8.2$ (where $\bar{S}$ is in %). The values of $\bar{S}$ were determined so that $\bar{r}$ would be larger than the minimal radii of the drop spectra.

The total mass of the nucleated drops is limited by the water vapor made available by the vapor field. If there was not enough vapor to nucleate all the CCN that could be activated at the particular supersaturation, the mass and concentration of the nucleated drops were reduced and renormalized. Consequently, the activated drops were converted back to CCN, starting with the smallest ones and continuing until the mass limitation was reached. The available mass is calculated according to (Soong 1974)

$$\delta M = \frac{\Delta S_w(t)}{A_w[P(t), T(t)]}, \tag{15}$$

where,

$$A_w[P(t), T(t)] = 1 + \frac{L}{c_p}\frac{dq_{s,w}}{dt}, \tag{16}$$

$\Delta S_w(t)$ is the specific humidity surplus with respect to water defined as the difference between the existing specific humidity and the specific humidity at saturation [see Eq. (B1)], and $q_{s,w}$ is the saturation specific humidity with respect to water.

The specific vapor perturbation and the supersaturation were recalculated after the depletion of water vapor by nucleation. The temperature was also updated following the release of latent heat.

2) Nucleation of ice particles

We parameterized the ice nucleation process by considering activation spectra of IN that depend on both the temperature and supersaturation with respect to ice, as given by Meyers et al. (1992). Accordingly, the number of ice crystals per liter nucleated at a certain temperature and supersaturation with respect to ice is

$$N_{i\bar{k}} = \exp[-2.8 + 0.262(T_0 - T)] + \exp(-0.639 + 0.1296S_i), \tag{17}$$

where $\bar{k}$ is the category of the initial size of the nucleated ice crystal (assumed to be 5 μm). The first term corresponds to the number of ice crystals predicted due to the contact freezing mechanism. Since aerosols scavenging was not modeled, it is implicitly assumed that all contact nuclei active at a certain temperature were immediately scavenged. Without a scavenging model, this term provides an upper bound to the number of ice crystals activated by contact nucleation. The second term accounts for the nucleation by deposition or condensation freezing. We assumed contact freezing nucleation to be active at temperatures colder than −2°C and deposition or condensation-freezing nucleation at temperatures colder than −5°C.

At each time step $N_{i\bar{k}}$ is calculated according to Eq. (17) and compared with the previous number of activated ice particles $N_{act\ ice}$. If $N_{act\ ice}$ is greater than $N_{i\bar{k}}$, no nucleation occurs; otherwise, $(N_{i\bar{k}} - N_{act\ ice})$ is the actual number of new ice crystals created. This procedure is similar to that applied by Clark (1974) for nucleation of drops. Subsequently, $N_{act\ ice}$ is updated,

and in the next time step the dynamic equation (4) is applied.

Because of the difficulties in quantitatively characterizing the Hallet–Mossop mechanism (Hallet and Mossop 1974) for secondary ice production, in terms of drop sizes, graupel sizes, temperature, and splinter sizes, we decided not to consider this process in the present model. This is a deficiency of the model that will be corrected in the future as more data becomes available. With this assumption we can expect the number of ice particles created at temperature $> -10°C$ to be somewhat underestimated, especially in maritime clouds. This deficiency is partly alleviated by taking into account processes such as nucleation by contact, condensation, and freezing, as well as the dependence of nucleation on supersaturation. In fact, our predicted ice concentrations were relatively high, especially at the warmer temperatures.

The available water vapor limitation is also applied here, similar to the case for nucleation of drops. The specific vapor perturbation and the supersaturation are updated appropriately.

3) DROP FREEZING

In this model graupel and ice crystals can be created by drop freezing. According to Bigg (1953), the number of frozen drops per unit time depends on the number of drops, their mass, and the supercooling:

$$\frac{dN_f(m,t)}{dt} = N_w(m,t)\frac{m}{\rho_w}\bar{A}\exp[\bar{B}(T_0 - T)], \quad (18)$$

where N_f is the number of frozen drops with mass m. The parameters $\bar{A}$ and $\bar{B}$ are equal to 10^{-4} cm^{-3} s^{-1} and 0.66 deg^{-1}, respectively, as those used by Orville and Kopp (1977). Accordingly, the number of frozen drops and their mass in category k during Δt ($t_0 \rightarrow t_0 + \Delta t$) is given by

$$N_{f_k} = N_{w_k}(t_0)\left\{1 - \exp\left[-\frac{\bar{m}_{w_k}}{\rho_w}\bar{A}\exp(\bar{B}\Delta T)\Delta t\right]\right\} \quad (19)$$

and

$$M_{f_k} = N_{f_k}\bar{m}_{w_k}. \quad (20)$$

In our model, frozen drops with radii greater than 100 μm are transferred to graupel or they are assigned to ice crystals (Alheit et al. 1990). At the end of each time step the temperature is recalculated according to the amount of latent heat released in the process.

4) DIFFUSIONAL GROWTH AND EVAPORATION OF DROPS AND ICE PARTICLES

The solution of the simultaneous diffusional growth (or evaporation) of drops and ice particles is based on Tzivion et al.'s (1989) solution for evaporation of water drops. The stochastic equation for condensation/evaporation of drops and/or for the deposition/sublimation of ice particles is of the form

$$\left.\frac{\partial n_y(m,t)}{\partial t}\right|_{\text{cond/evap, sublim/depos}} = -\frac{\partial}{\partial m}\left[n_y(m,t)\left(\frac{dm}{dt}\right)_{\text{cond/evap, depos/sublim}}\right], \quad (21)$$

where $y = w, i, g, s$ (drops, ice particles, graupel, and snow, respectively). The rate of change of mass for a single particle is given by

$$\left(\frac{dm}{dt}\right)_{\text{cond/evap, sublim/depos}} = C_{w/x}[P(t), T(t)]\Delta S_{w/i}(t)m^{1/3}, \quad (22)$$

where we have neglected curvature and solute effects.

Here, $\Delta S_{w/i}$ (the specific humidity surplus with respect to water and ice, respectively); P, T (pressure and temperature, respectively); and n_y are also functions of (z, r). Where $C_{w/x}(P, T)$ are known functions of P and T for water (w) and ice particles ($x = g, i, s$), as given by Pruppacher and Klett (1978):

$$C_w(P,T) = \left(\frac{3}{4\pi\rho_w}\right)^{1/3} \times \frac{4\pi f_{v,w}}{q_{s,w}\left[\frac{L}{k_aT}\left(\frac{L}{R_vT} - 1\right) + \frac{R_vT}{D_ve_{\text{sat},w}}\right]} \quad (23)$$

and

$$C_x(P,T) = \frac{4\pi C_x^* f_{v,i}}{q_{s,i}\left[\frac{L_{vi}}{k_aT}\left(\frac{L_{vi}}{R_vT} - 1\right) + \frac{R_vT}{D_ve_{\text{sat},i}}\right]}. \quad (24)$$

The ventilation factor for drops is given by

$$f_{v,w} = \begin{cases} 1.00 + 0.108\chi^2, & \chi = N_{\text{Sc}}^{1/3}N_{\text{Re}}^{1/2} < 1.4 \\ 0.78 + 0.308\chi & \chi \geq 1.4 \end{cases} \quad (25)$$

and for ice particles by

$$f_{v,i} = \begin{cases} 1.00 + 0.14\chi^2, & \chi = N_{\text{Sc}}^{1/3}N_{\text{Re}}^{1/2} < 1.0 \\ 0.86 + 0.28\chi^2 & \chi \geq 1.0, \end{cases} \quad (26)$$

both after Pruppacher and Klett (1978).

In Eq. (24), C_x^* is the shape factor of the ice particles (oblate spheroid for ice crystals, spheroid for graupel and snow), expressed as a coefficient of $m^{1/3}$. The Reynolds number (N_{Re}) for the ice crystals is defined in terms of the characteristic length L^*, which is the ratio

of the total surface area of the particle to the perimeter of the area projected normal to the flow direction. The relationship between the thickness and the diameter of the unrimed ice crystals is calculated based on Auer and Veal (1970). The other parameters are defined in appendix A.

The analytical solution of Eq. (21) for a single time step Δt is given by (Tzivion et al. 1989)

$$n_y(m, t + \Delta t) = \frac{1}{m^{1/3}}\left[\left(m^{2/3} - \frac{2}{3}\tau_{w/x}\right)^{1/2}\right] \times n_y\left[\left(m^{2/3} - \frac{2}{3}\tau_{w/x}\right)^{3/2}, t\right]. \quad (27)$$

We assume that $C_w(P, T)$ and $C_x(P, T)$ remain constant during Δt and that

$$\tau_{w/x} = C_{w/x}(P, T)\int_t^{t+\Delta t} \Delta S_{w/i}(t)dt. \quad (28)$$

The moments N_{y_k} and M_{y_k} in each category can be calculated at time $t + \Delta t$ according to Eqs. (8) and (9), respectively:

$$N_{y_k}(t + \Delta t) = \int_{z_k}^{z_{k+1}} n_{y_k}(m, t)dm \quad (29)$$

$$M_{y_k}(t + \Delta t) = \int_{z_k}^{z_{k+1}} \left[m^{2/3} + \frac{2}{3}\tau_{w/x}\right]^{3/2} n_{y_k}(m, t)dm, \quad (30)$$

where

$$z_k = \left[x_k^{2/3} - \frac{2}{3}\tau_{w/x}\right]^{3/2}; \quad z_{k+1} = \left[x_{k+1}^{2/3} - \frac{2}{3}\tau_{w/x}\right]^{3/2}. \quad (31)$$

In order to calculate $\tau_{w/x}$, we have to solve the integral of ΔS_w and ΔS_i for one time step. The expressions for the integrals of the supersaturations are given by integration of Eqs. (B27) and (B28) in appendix B:

$$\int_t^{t+\Delta t} \Delta S_w(t)dt = \Delta S_w \Delta t - \left(\frac{\Delta t}{R_w + R_i}\right)[R_w \Delta S_w + P_i \Delta S_i]\left\{1 - \frac{\{1 - \exp[-(R_w + R_i)\Delta t]\}}{(R_w + R_i)\Delta t}\right\} \quad (32)$$

and

$$\int_t^{t+\Delta t} \Delta S_i(t)dt = \Delta S_i \Delta t - \left(\frac{\Delta t}{R_w + R_i}\right)[P_w \Delta S_w + R_i \Delta S_i]\left\{1 - \frac{\{1 - \exp[-(R_w + R_i)\Delta t]\}}{(R_w + R_i)\Delta t}\right\}, \quad (33)$$

where $R_{w/i}$ and $P_{w/i}$ are defined in appendix B.

From these last two equations we can see that when drops and ice particles grow (or evaporate) simultaneously the supersaturations with respect to water and to ice depend on the concentration and average mass of the drops and ice particles present. As a special case, when the temperature is warmer than 0°C or when no ice is present at $T < 0$°C, R_i and P_i are zero, and Eq. (32) becomes the original equation for $\int \Delta S_w dt$, as appears in Tzivion et al. (1989).

During condensation, $\Delta S_w(t + \Delta t)$ can change its sign within one time step. During diffusional growth, the supersaturations with respect to water and to ice steadily decrease until water saturation is reached, at which point ice particles continue to grow by deposition and water vapor pressure continues to decrease. At the same time, water drops begin to evaporate because the water vapor pressure is subsaturated with respect to water (ice particles grow by the Bergeron–Findeisen process). Thus, within one time step there is a switch from condensation to evaporation of the water drops. Therefore, in case $\Delta S_w > 0$, we calculate Δt_w^* (the time required for the specific humidity surplus with respect to water to change its sign and become negative) from Eq. (B29) (see appendix B); if $\Delta t_w^* < \Delta t$ (and positive), we split the calculation within one time step: Δt_w^* is used to calculate the growth of drops and ice particles, and $\Delta t - \Delta t_w^*$ is used for the evaporation of the drops and the growth of the ice particles. A similar process may occur when sublimation of ice can switch over to deposition. The time step Δt used for these processes is 2.5 s.

Since in the model we did not follow the number, size, or type of the nuclei (CCN or IN) inside the hydrometeors, we have no way of knowing what kind of particles are released after evaporation. Subsequently, the model does not consider the recycling of CCN or IN. In separate tests conducted with a warm cloud (only CCN) we found that the recycling of CCN has very little influence on the rain formation processes in the type of convective clouds simulated here.

5) MELTING OF ICE PARTICLES

Melting is a difficult process to treat accurately in a numerical model because water and ice can coexist in the same particle. However, this process cannot be ignored since it influences a number of important variables, by cooling the air, producing downdrafts, affecting the fall speed of the particles by changing their density, changing the particle size distribution by shedding melted water from the ice particles, and affecting the collision efficiencies of the particles. Usually, melting is crudely parameterized by assuming that ice instantaneously melts at the 0°C isotherm (Khvorostyanov et al. 1989) or some distance below. In this last case the melting distance is calculated based on the time required for the complete melting of the particle and on its velocity (Takahashi 1976). Recently, Walko et al. (1995) introduced in the Colorado State Univer-

sity Regional Atmospheric Model System a thermodynamic parameter used to diagnose the degree of melting of the ice particles. This formulation, however, is not included in the present model.

Melting of ice particles is treated in our model in a way similar to evaporation. The stochastic equation for melting is

$$\left.\frac{\partial n_x(m,t)}{\partial t}\right|_{\text{melting}} = -\frac{\partial}{\partial m}\left[n_x(m,t)\left(\frac{dm}{dt}\right)_{\text{melting}}\right], \tag{34}$$

where $n_x(m, t)$ represents the distribution function for one of the ice species and

$$\left(\frac{dm}{dt}\right)_{\text{melting}} = I(P,T)m^{1/3}. \tag{35}$$

As given by Rassmussen and Heymsfield (1987), $I(P, T)$ is a function of pressure and temperature:

$$I(P,T) = \begin{cases} \left(\dfrac{6\pi^2}{\rho_i}\right)^{1/3} \dfrac{K_a}{L_{iw}} 2\bar{f}_h(T_0 - T), \\ \qquad N_{\text{Re}} < 6 \times 10^3 \\ \left(\dfrac{6\pi^2}{\rho_i}\right)^{1/3} \dfrac{K_a}{L_{iw}} \chi N_{\text{Re}}^{1/2} N_{\text{Pr}}^{1/3}(T_0 - T), \\ \qquad N_{\text{Re}} \geq 6 \times 10^3, \end{cases} \tag{36}$$

where K_a is the thermal diffusivity; N_{Re} and N_{Pr} are the Reynolds and Prandtl numbers, respectively; $\bar{f}_h$ is the ventilation factor given by

$$\bar{f}_h = 0.78 + 0.308 N_{\text{Pr}}^{1/3} N_{\text{Re}}^{1/2}; \tag{37}$$

and χ is 0.74 if $N_{\text{Re}} \leq 2 \times 10^4$ or $\chi = 0.57 + 9 \times 10^{-6} N_{\text{Re}}$, otherwise.

By assuming that the temperature T remains constant during one time step, the analytical solution to Eq. (35) becomes similar to Eq. (27), $(I(P, T) < 0)$:

$$n_x(m, t + \Delta t) = \frac{1}{m^{1/3}}\left\{\left[m^{2/3} + \frac{2}{3} I(P,T)\Delta t\right]^{1/2}\right\} \times n_x\left\{\left[m^{2/3} + \frac{2}{3} I(P,T)\Delta t\right]^{3/2}, t\right\}. \tag{38}$$

Equations for the moments in the category are similar to Eqs. (29)–(31), where $\tau = I(P, T)\Delta t$.

After calculating the mass of ice that melted during one time step, we shed this mass to form two drops of equal mass [inspired by the description in Rasmussen and Heymsfield (1987)]. If the mass of these created drops is smaller than the lower limit of the first category, we still put them into the first category but normalize the number concentration to ensure mass conservation. We recognize that the parameterization describing the redistribution of the shedded drops from the melted ice particles is crude. But unfortunately, there are no consistent and reliable experimental data that could be used. In addition, in the model the size distribution of the shedded drops depends on the integration time step, because the mass of the melted ice also depends on the same time. Fortunately, melting becomes important when big hydrometeors are already present, so that rain formation is not seriously affected by this parameterization.

6) DROP–DROP, ICE–ICE, ICE–DROP INTERACTIONS AND BREAKUP OF DROPS

The model considers collisional coagulation between the different species, as well as collisional breakup of drops. These interactions can lead to the transformation from one particle type to another. We made the following assumptions.

1) Snow particles are formed and grow by aggregation of ice crystals.
2) Ice crystals can grow by riming with drops smaller than themselves as long as the overall rimed mass is less than the mass of the ice crystal itself (or a certain fraction of it); otherwise, the ice crystal becomes a graupel particle.
3) The interactions between graupel and other particles always produce graupel.
4) Graupel is also created by drops that collide with snow particles and ice crystals smaller than themselves.

A summary of the different particle interactions is presented in Table 1. Using the stochastic collision equation, gain and loss terms are formulated according to the interactions indicated in Table 1, and a set of

TABLE 1. Summary of ice–ice and ice–drop interactions. The gain and loss columns are for a specific category k.

	Gain	Loss
Drops	drops + drops	drops + drops
		drops + ice
		drops + snow
		drops + graupel
Ice	ice + drops ($m_i > m_w$)	ice + ice
		ice + drops
		ice + snow
		ice + graupel
Snow	ice + ice	snow + snow
	snow + snow	snow + drops
	snow + ice	snow + ice
	snow + drops ($m_s > m_w$)	snow + graupel
Graupel	graupel + graupel	graupel + graupel
	graupel + snow	graupel + drops
	graupel + ice	graupel + ice
	graupel + drops	graupel + snow
	snow + drops ($m_w > m_s$)	
	ice + drops ($m_w > m_i$)	

four equations is obtained for the four distribution functions of the different species (see appendix C). These equations are transformed into moment equations, yielding a set of equations for the specific mass and number of the different particles. Using the method of multimoments, these equations can be solved based on the solution presented by Tzivion et al. (1987) and Feingold et al. (1988). The complication here is that, due to the interaction of particles of different type, particles may lose their identity and become members of a different species (e.g., a big drop collides with a small graupel and becomes a big graupel). For this reason, the equations for the moments of the different species must be separated into exact gain and loss terms to ensure overall mass conservation. An example of the algorithm for this process is shown in appendix C.

The kernel of Low and List (1982a,b) was used for raindrops larger than 0.6 mm. In the region 0.1–0.6 mm, the coalescence efficiencies of Ochs et al. (1986) were employed as collection efficiencies (assuming that the collision efficiencies in this range are close to unity). The work of Ochs et al. covers the range 0.1–0.3 mm, but due to lack of better data, we assume that their results can be extended to 0.6 mm. For smaller droplets the collision efficiencies of Long (1974) were adapted.

The collision efficiencies between graupel and drops were calculated according to Hall (1980) and Rasmussen and Heymsfield (1985). The available experimental and theoretical data on the collision efficiencies between ice crystals and drops are rather scarce. For ice crystals (plates) colliding with drops we used the collision efficiencies given by Martin et al. (1982) and for large supercooled drops colliding with planar ice crystals we used the coefficients calculated by Lew et al. (1985). The data for collision efficiencies as given by Martin et al. (1982) do not cover the full range of ice particles and drop sizes required by the model. The data can be mathematically extrapolated for the whole range, resulting in unrealistically very low efficiencies for large ice particles colliding with smaller drops. Chen (1992) suggested a different approach to fill the gaps in the data. The collision efficiencies reach a minimum for similar terminal velocities of the colliding ice particle and drop, after which the coefficients grow because the difference in terminal velocities changes sign and increases. One can consider that the efficiencies behave in a similar way to those of large drops colliding with smaller ice crystals, as given by Lew et al. (1985). These two different approaches produce very different results for the kernel of the interactions. The simple extrapolation produced unrealisticly low rates of riming. This was especially true for large ice crystals that continued to grow by deposition but not by riming, preventing them from becoming graupel. Rain was not produced in continental clouds (for CCN concentrations higher than 900 cm^{-3} at 1% supersaturation) or it began only after almost 2 h of cloud simulation. Consequently, the collision efficiencies were corrected to those proposed by Chen (1992). Coalescence efficiencies for interactions between ice–ice, ice–snow, ice–graupel, snow–snow, snow–graupel, and graupel–graupel were used in accordance with Wang and Chang (1993), in which the dependence on temperature was considered.

7) SEDIMENTATION OF DROPS AND ICE PARTICLES

The equation for sedimentation is given by

$$\frac{\partial n_x(m, z, r, t)}{\partial t} = -\frac{\partial}{\partial z}[n_x(m, z, r, t)v_x(m, z)]. \tag{39}$$

The fall velocity of drops is given by

$$v_w(m, z) \Rightarrow v_{w_k}(z) = \alpha_k \bar{m}_k^{\beta_k}\left[\frac{\rho_a(z=0)}{\rho_a(z)}\right]^{0.4}, \tag{40}$$

where $\bar{m}_k$ is the average mass in category k, (α, β) are drop mass-dependent parameters according to Beard (1976), and ρ_a is the air density.

The terminal fall velocities for the ice particles are calculated according to Böhm's (1989) formulation:

$$v_x(m, z) \Rightarrow v_{x_k}(z) = \frac{\mathrm{Re}\eta}{2\rho_a(z)}\left(\frac{\pi}{A_{x_k}}\right)^{1/2}, \tag{41}$$

where

$$\mathrm{Re} = 8.5[(1 + 0.1519X^{1/2})^{1/2} - 1]^2 \tag{42}$$

and

$$X = \frac{8m_k g\rho_a}{\pi\eta^2}\left(\frac{A_{x_k}}{A^*_{x_k}}\right)^{1/4}. \tag{43}$$

In Eq. (43), $A^*_{x_k}$ is the effective projected area presented to the flow by an ice particle of type x with mass m_k, and A_{x_k} is the circumscribed area defined as the area of the smallest circle or ellipse that completely contains $A^*_{x_k}$; η is the kinematic viscosity.

From Eqs. (39), (8), and (9), we get advection-type equations for M_{x_k} and N_{x_k}. We solve them using the positive-definite advection scheme of Smolarkiewicz (1983) in order to minimize numerical diffusion.

3. Results

We present here the results obtained for a test case on a continental cloud.

The initial conditions were given by a theoretical profile of temperature and relative humidity as shown in Fig. 2 (dewpoint is plotted instead of relative humidity). The temperature and pressure at the surface were 16°C and 1007 hPa. For initialization, a pulse of heat that produced a 2°C perturbation was applied for one time step at $t = 0$ at a height of 600 m, 150 m off the axis.

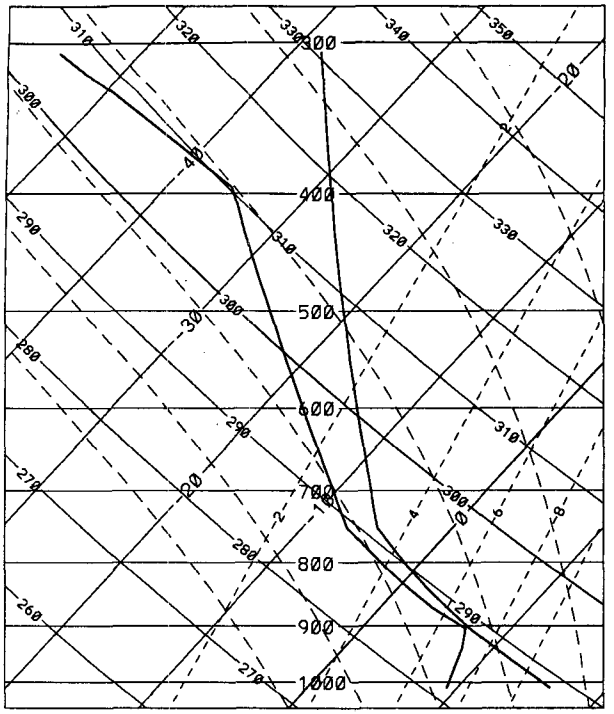

FIG. 2. Vertical profiles of temperature and dewpoint.

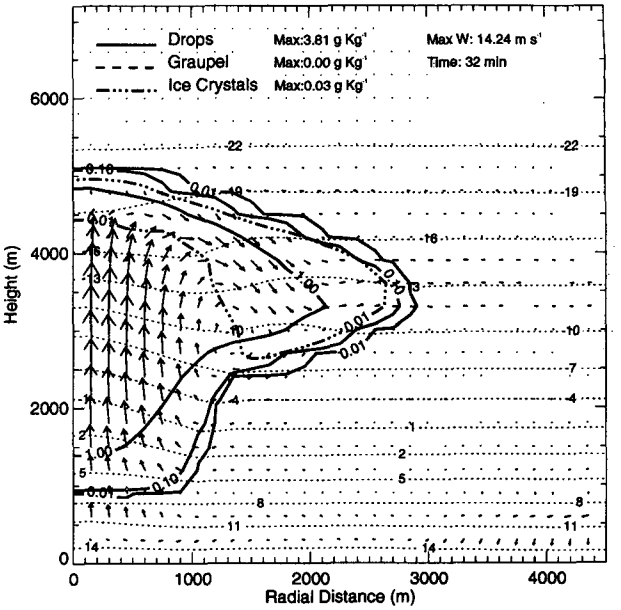

FIG. 3. Contours of equal mass content (g kg^{-1}) for drops, graupel and ice crystals, and wind vectors (m s^{-1}) 32 min from model initiation (22 min from cloud formation) at the stage of maximum dynamic development. The horizontal dashed lines are isotherms.

The nucleated drops were distributed according to an exponential function with average radii of 3 μm. The parameters of the activation spectra were N_0 = 900 cm^{-3} and α = 0.8, characteristic of continental clouds. The model was run until the maximum rain rate decreased below 1 mm h^{-1} (80 min).

Ten minutes after model initialization a cloud began to form. The vertical velocity at cloud axis rapidly increased and reached a maximum of 14 m s^{-1} at 3000-m height, 22 min from cloud formation (Fig. 3). At that time the liquid water content (LWC) also reached its maximum value of 3.8 g kg^{-1} at 4200-m height. The ice crystal mass content at this stage was less than 0.03 g kg^{-1}, and the graupel mass content was negligible. In Fig. 3, contours of the drop, graupel, and ice crystal mass content are displayed on the background of the wind field, at the time (32 min) of maximum dynamic development. The cloud base was at 1200 m at 5°C, and the cloud top at 4800 m (defined as the place where the relative humidity decreased below 100%); the temperature was −19°C, and the 0°C isotherm was located at around 1800 m (700 m above cloud base).

Following this stage, the growth of ice accelerated, and intense riming began. Figure 4 presents the contours of the drop, graupel, and ice mass content during the mature stage, 40 min from model initiation, when the graupel mass content exceeded the ice mass content and drizzle began. The updrafts at the cloud axis were still vigorous (11.5 m s^{-1}), but downdrafts began at the cloud edge. At this stage the maximum graupel and ice mass content were located about 1 km off the cloud axis, while the maximum LWC was right at cloud axis.

The decay stage of the cloud is depicted in Fig. 5. Fifty-two min from model initiation, rain reached its

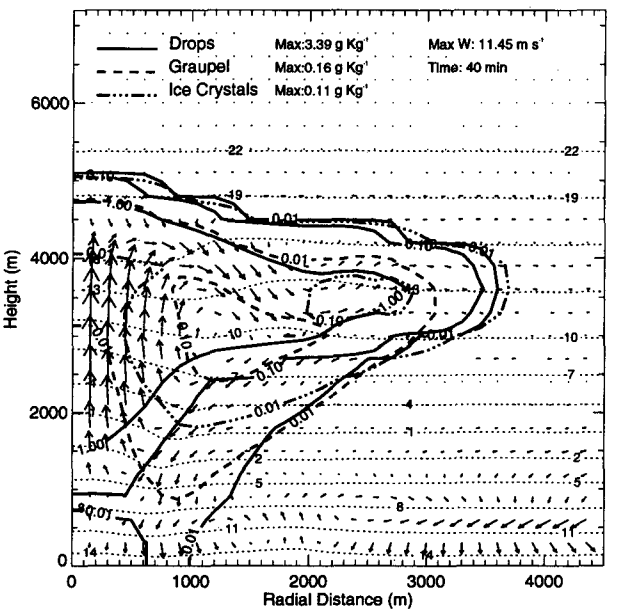

FIG. 4. Contours of equal mass content (g kg^{-1}) for drops, graupel and ice crystals, and wind vectors (m s^{-1}) 40 min from model initiation (30 min from cloud formation) during the mature stage of the cloud. The horizontal dashed lines are isotherms.

maximum intensity: 24 mm h^{-1} at cloud axis and 26 mm h^{-1} 300 m off the axis. The downdrafts at cloud axis were also at their maximum: -15.4 m s^{-1}. While the graupel mass content reached its maximum value of almost 1 g kg^{-1}, the LWC decreased significantly to 0.61 g kg^{-1}, a decrease that stemmed mainly from riming, collection by graupel, and rain washout. The drastic reduction in water content resulted in a decrease in the riming process and a slowdown of mass growth of the ice crystals.

Figure 6 shows that as the cloud approached the stage of complete dissipation (72 min from model initialization) it remained almost completely glaciated, with ice mass loading of 0.6 g kg^{-1}, a smaller amount of graupel (0.3 g kg^{-1}), and a very small pocket of LWC close to cloud top. A small amount of water from the melting of ice particles formed below 2000 m. At this stage, rain intensity rapidly decreased to below 2 mm h^{-1}.

Ice crystals appeared as soon as the cloud top reached the -5°C level, ≈15 min from model initiation. Figure 7 shows the contours of ice crystals and graupel number concentration at four different times (as in Figs. 3–6). At the stage of maximum development, ice crystal concentration reached its maximum value of 16 L^{-1}, at a height of ~4000 m (-16°C), at a time when graupel concentration was less than 0.01 L^{-1}. During the mature stage, the graupel concentration rapidly increased to 0.6 L^{-1} at 40 min. This maximum was located directly below the maximum of the ice crystals concentration, ≈2 km off the cloud axis, at a temperature of -10°C. A maximum graupel concentration of 1 L^{-1} was obtained during the decay stage (52 min) at 1800-m height (very close to the 0°C isotherm), ~1000 m off the cloud axis. The ice crystal concentration decreased to half its maximum, 8 L^{-1}. Close to the final dissipation stage (72 min) graupel descended to the lower parts of the cloud.

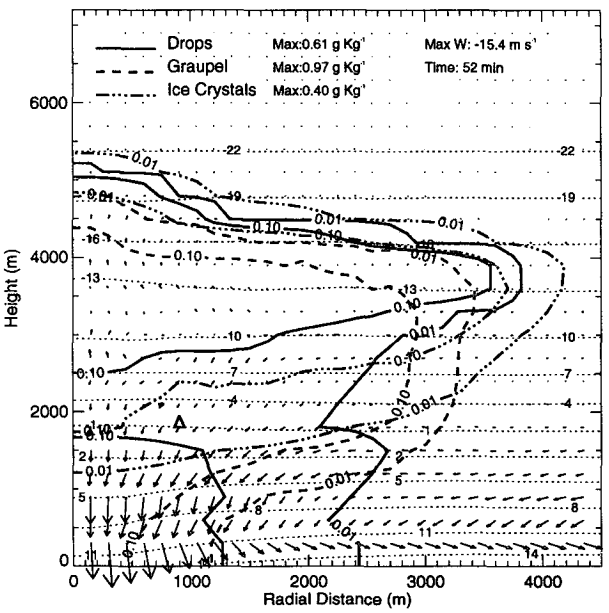

FIG. 5. Contours of equal mass content (g kg^{-1}) for drops, graupel and ice crystals, and wind vectors (m s^{-1}) 52 min from model initiation (42 min from cloud formation) during the decay stage of the cloud. The horizontal dashed lines are isotherms.

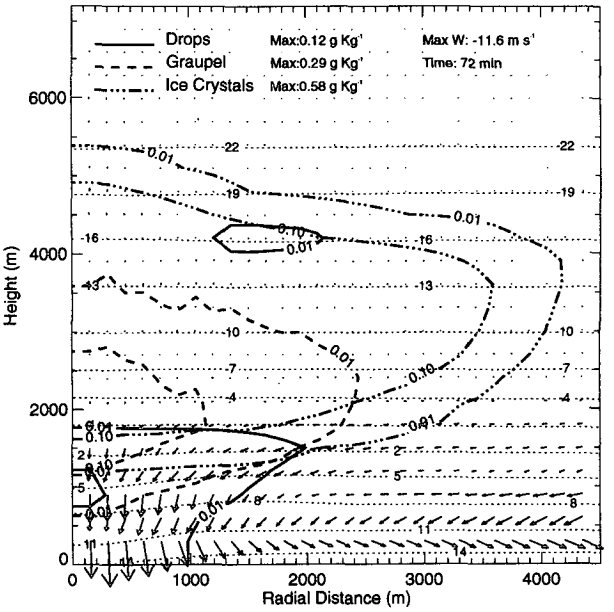

FIG. 6. Contours of equal mass content (g kg^{-1}) for drops, graupel and ice crystals, and wind vectors (m s^{-1}) 72 min from model initiation (62 min from cloud formation) during the final dissipation of the cloud. The horizontal dashed lines are isotherms.

At the end of the simulation, the accumulated rain at cloud axis was 4.6 mm and reached a maximum of 5.1 mm at 300 m off the axis, beyond which the rain sharply decreased to almost negligible amounts at 1 km off the axis. The rain began 30 min after cloud formation and rapidly increased in intensity; the major fraction of the rain fell between 48–58 min from cloud initiation.

Figure 8 illustrates the total mass in the cloud for the different particle types as a function of time, normalized with respect to maximum LWC. The total LWC in the cloud reached its maximum value 36 min from model initialization, at which time the total mass of the ice crystals was 1% that of the drops and the graupel mass was less than 0.3%. At the same time, the total mass loading (water + ice crystals + graupel + snow) of the cloud reached its maximum. After this time the amount of water and ice mass that evaporated or precipitated exceeded the amount of mass condensated on drops or ice particles inside the cloud. The graupel mass rapidly increased as a result of graupel production by riming and drops freezing. Twenty-four minutes later, most of the cloud mass (30% of the maximum LWC) was in the form of graupel, while

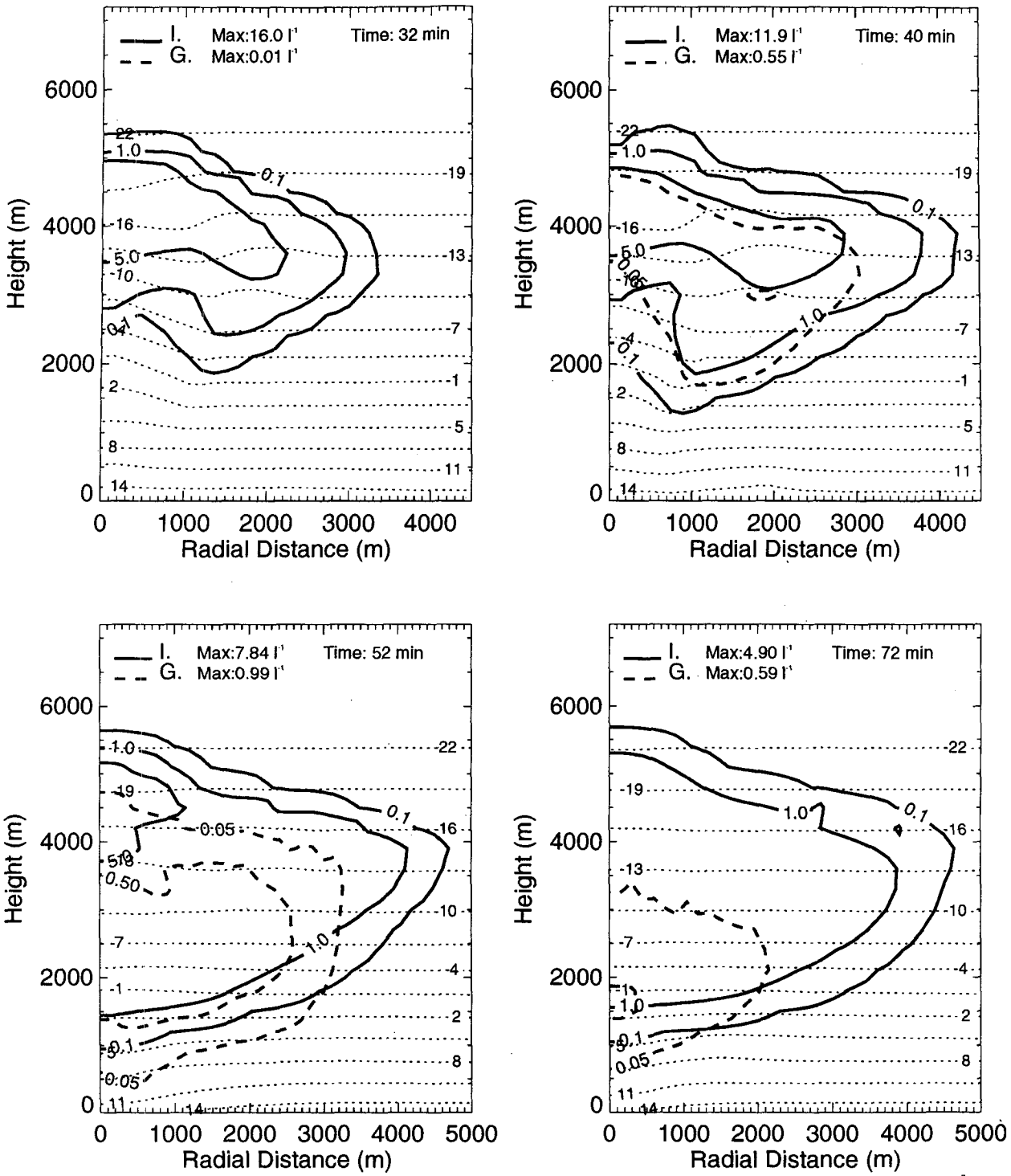

FIG. 7. Contours of equal number concentration (L^{-1}) for graupel and ice crystals at 32, 40, 52, and 72 min from model initiation. The horizontal dashed lines are isotherms.

the drops mass content composed only 20%, and the ice crystal mass about 12%. After the period of heavy rain, the total mass of the ice crystals became predominant and constituted 25% of the maximum LWC, the drops and graupel mass content were significantly depleted (no more than 0.7%), and the snow mass stead-

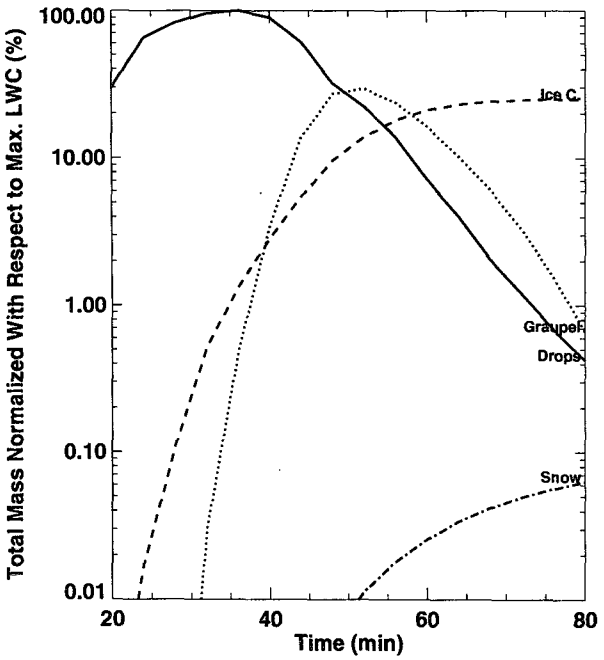

FIG. 8. Percent of the total mass for each species normalized with respect the maximum LWC, as a function of time.

ily increased but never reached even 0.1% of the maximum LWC.

Analysis of the distribution functions

Distribution functions for the mass and number concentrations of the drops are shown in Fig. 9 at 150 m from cloud axis, 3000-m height (−10°C), and at seven different times during the mature and decay stages of the cloud. In terms of number density, the spectrum remained rather narrow, and drops larger than 100 μm in diameter were not produced in significant concentrations. The mass distributions did reveal, however, that a bimodality developed through the collision–coalescence process (Bleck 1970; Tzivion et al. 1987), especially at 3000 m. As was already pointed out, the concentrations of these large drops were very low compared to the total number concentration of the drops. Similar plots but at the 1200-m level are shown in Fig. 10. Here, the small drops were depleted as soon as rain began and big drops appeared. It should be noted that big drops already appeared at 36 min, 1350 m off the cloud axis (not shown), confirming that the rain spread from the outer parts of the cloud toward the axis, as mentioned before. The different peaks seen in the raindrops range at 1200 m were partly created by the shedded water from the melting of ice particles.

The distribution functions for the ice particles are shown in Fig. 11 at 150 m from cloud axis, 4200-m height (−17°C), at the same times as Fig. 9. The peak at the smaller sizes (~10 μm), especially at the earlier times, was related to the recent nucleation on IN. Later on when most IN were depleted, this peak vanished. The other peaks in the number concentration spectra that appear at higher elevations resulted from the ascent of ice particles that were nucleated below and accumulated mass in the updraft. Some of the ice was due to the contribution from frozen small drops. From both mass and number distributions it can be seen that during the stage of intense riming (36–52 min) ice crystals did not exceed the 1000-μm diameter. This is because at these sizes many of the ice crystals were converted to graupel. When the number of drops was depleted, riming became ineffective and graupel production stopped (~52 min), enabling ice crystals to continue to grow by vapor deposition. At 1200-m height (not shown) a distinct spectrum of melting particles was observed, down to

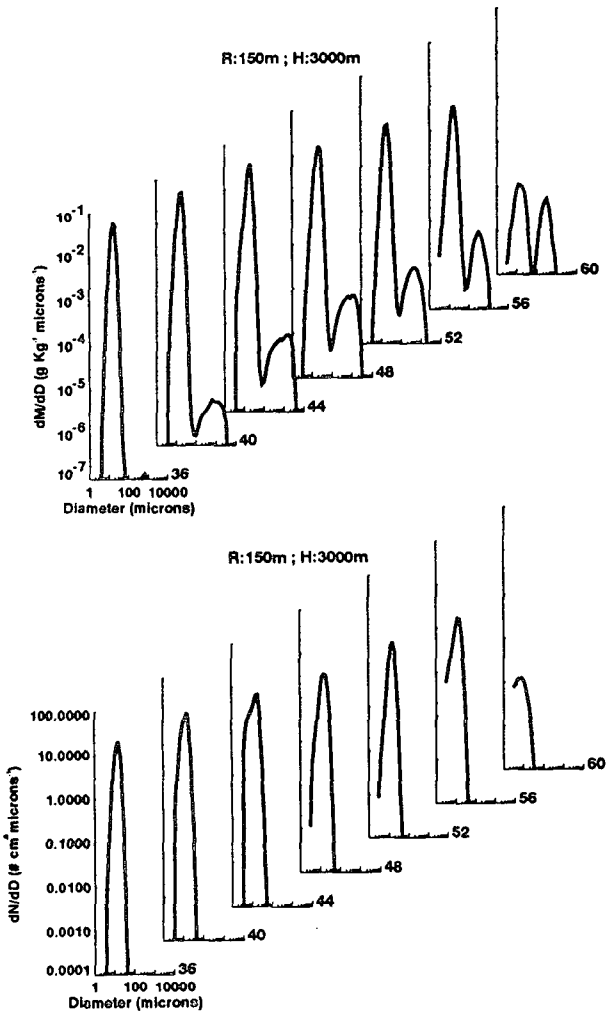

FIG. 9. Mass (top) and number (bottom) concentration distribution functions for drops at 150 m from cloud axis, 3000-m height (≈ −10°C), and at different times (in min).

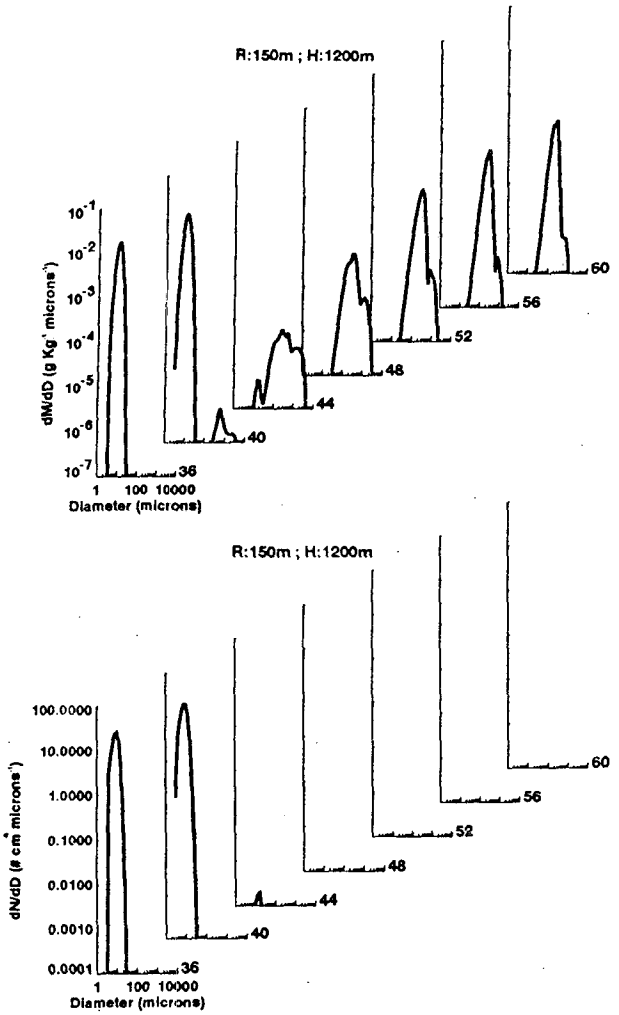

FIG. 10. As in Fig. 9 except at 1200-m height.

very small sizes corresponding to particles that did not completely melt.

The graupel spectra, shown in Fig. 12 for the same location and times as Fig. 11, show that particles appeared at sizes where the ice crystals abruptly terminated, indicating that graupel particles were mainly produced by riming of ice crystals. As can be seen, graupel reached very big sizes. The general shape of the distribution obtained for the graupel at 1200 m (not shown) was somewhat similar to that obtained for the ice particles, except that the sizes of the graupel particles were much greater. This led to the graupel mass being greater by more than one order of magnitude than the ice mass.

Snow particle distributions are not shown since their number and mass concentrations were several orders of magnitude lower than those of ice crystals or graupel. Snow particles did not play a significant role in the formation of rain in the convective cloud simulated in this case.

4. Summary and conclusions

An axisymmetric cloud model with detailed microphysics for both warm and cold processes was presented. The model is unique for many reasons.

1) All processes are formulated using the method of moments, and two physical moments of the distribution functions are calculated: number and mass concentration.

2) The processes of diffusional growth, collision–coalescence, collisional breakup, and melting are solved with stochastic equations.

3) The diffusional growth in the mixed phase (vapor–water–ice) is calculated simultaneously for drops and ice particles, which means that the supersaturation with respect to both ice and water can be solved with relatively high accuracy.

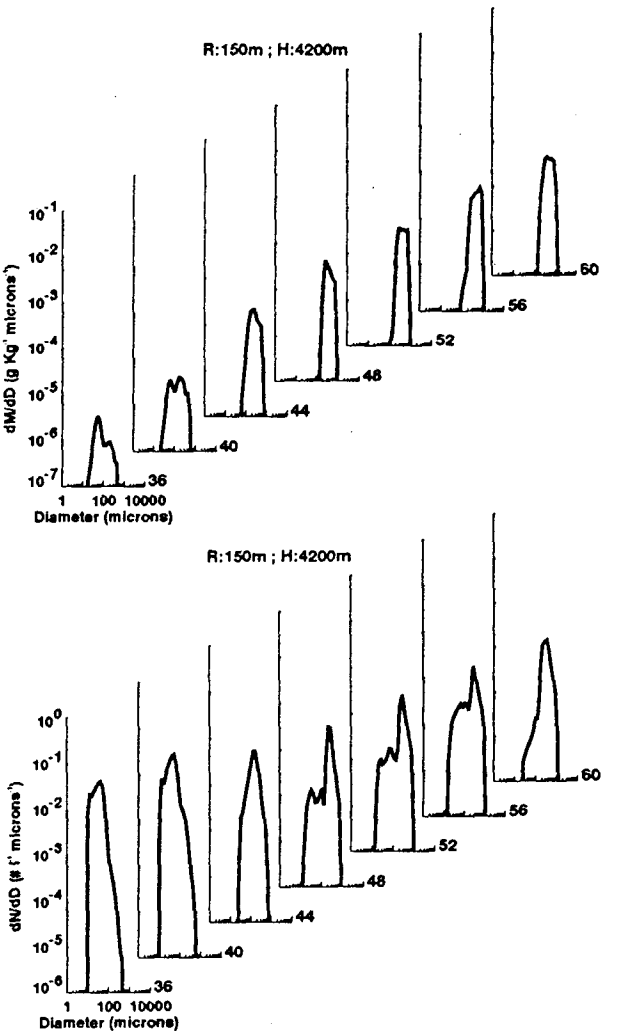

FIG. 11. Mass (top) and number (bottom) concentration distribution functions for ice crystals at 150 m from cloud axis, 4200-m height (~ −17°C), and at different times (in min).

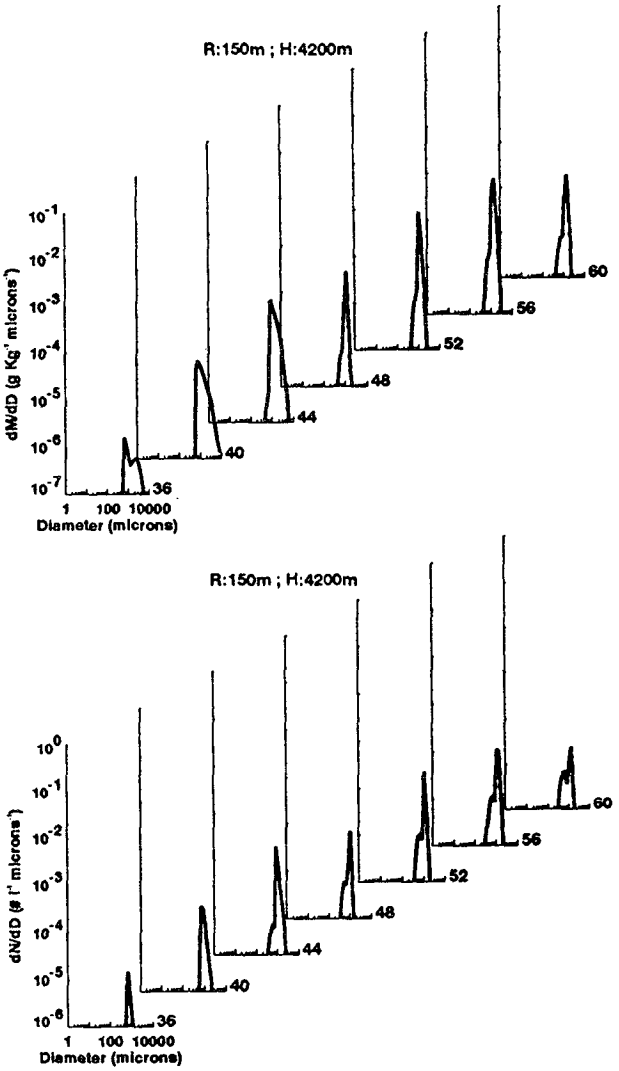

FIG. 12. Mass (top) and number (bottom) concentration distribution functions for graupels at 150 m from cloud axis, 4200-m height (~ −17°C), and at different times (in min).

4) The collisional coalescence between ice–ice and ice–drops is formulated such that the overall mass is conserved and the changes in number concentrations are explicitly calculated independent from the mass concentration (in contrast to the one-moment methods).

5) The scheme for drop nucleation is inexpensive in computing time and provides a good parameterization by considering a distribution function for the activation of CCN as a function of supersaturation.

The simulation of a continental cloud demonstrated the ability of the model to simulate rain formation processes in convective clouds. Drop growth by condensation and coagulation, ice initiation by nucleation or drop freezing, riming and subsequent production of graupel were efficiently simulated. The effects of melting of ice particles on the precipitation and sedimentation of other hydrometeors were also considered. Analysis of mass and number concentration distribution functions provides an important insight into the microphysical processes involved in rain formation.

One of the important things that came out of the present simulation is that at the time of rain formation, even though ice particles grow very rapidly by diffusion, their low concentrations do not reduce the humidity to below water saturation and, therefore, do not lead to drop evaporation, in contrast to that predicted by the Bergeron–Findeisen mechanism (Cotton and Anthes 1989).

Part II of this work will compare the results of simulations carried out with different initial spectra of drops and ice particles. The main processes involved in rain formation in maritime and continental clouds will be inferred from the results.

Acknowledgment. We would like to thank Mekorot Water Company of Israel and its subsidiary, E.M.S, for partially funding this research. Thanks are also due to Mr. and Mrs. L. Ross for their contribution to the laboratory, which made part of this work possible.

APPENDIX A

Definitions of Symbols Used in the Model

All units are in mks, unless otherwise stated.

A, B	functions of the parameters and average radius of the distribution function of newborn drops
$\bar{A}, \bar{B}$	parameters used in the formula for drop freezing
$A_w(P, T); A_i(P, T)$ $C_w(P, T); C_x(P, T)$	known functions of pressure and temperature
$A^*_{x_k}$	effective projected area presented to the flow by an ice particle of type x and mass m_k
A_{x_k}	area of the smallest circle or ellipse that completely contains $A^*_{x_k}$
$B(x, y)$	breakup kernel between drops with masses x and y
c_p	specific heat at constant pressure
C^*_x, L^*	shape factor and characteristic length for the ice particles, respectively
C_t	constant
$C_{a,b}(x, y)$	collection kernel between particles of type a and b
$C_{k,i}$	approximation of the collection kernel for categories k and i
D	advection operator

D_v	molecular diffusion coefficient
$e_{sat,w}$; $e_{sat,i}$	vapor pressure at saturation with respect to water and ice, respectively
$E(x, y)$	collection efficiency for particles with mass x and y
$f_{v,w}$; $f_{v,i}$	ventilation factor for drops and ice, respectively
f_i	ventilation factor for ice melting
$f(r)$	distribution function of the newborn drops
F_g	turbulence operator
$\mathcal{F}_k$	a function of the supersaturation in category k
g	magnitude of acceleration of gravity
$GN_{(a,b),k}$; $GM_{(a,b),k}$	gain terms at category k due to interaction between particles of type a and b for the specific number and mass, respectively
GN, GM	gain terms for the specific number and mass, respectively
H, R	upper and lateral boundary, respectively
J, J_{CCN}	number of categories for the cloud particles and the CCN, respectively
k	index for the number of the category
k_a	coefficient of thermal conductivity of air
$\bar{k}$	category number of the initial size of the nucleated ice crystal
K_a	coefficient of thermal diffusivity
$K(x, y)$	gravitational geometric collection kernel for particles with masses x and y
m	mass
m_k, x_k	mass of the beginning of category k
$\bar{m}_k$	average mass in category k
L, L_{vi}, L_{iw}	latent heat of condensation, sublimation, and melting, respectively
$LN_{(a,b),k}$; $LM_{(a,b),k}$	loss terms at category k due to interaction between particles of type a and b for the specific number and mass, respectively
LN, LM	loss terms for the specific number and mass, respectively
M_k	specific mass content in category k
M_k^j	moment j of the distribution function in category k
M_{w_k}, M_{i_k}, M_{g_k}, M_{s_k}	specific mass content in category k for drops, ice, graupel, and snow, respectively
M_{f_k}	specific mass of frozen drops in category k
n_i, g_i	in appendix C, the mass distribution function for drops and graupel at category i, respectively
$n_i(m, z, r, t)$	ice size distribution function with respect to mass m, at location (z, r) and time t
$n_g(m, z, r, t)$	graupel size distribution function with respect to mass m, at location (z, r) and time t
$n_s(m, z, r, t)$	snow size distribution function with respect to mass m, at location (z, r) and time t
$n_w(m, z, r, t)$	drop size distribution function with respect to mass m, at location (z, r) and time t
N_k	specific number in category k
N_{w_k}, N_{i_k}	specific number in category k for drops, ice, graupel,
N_{g_k}, N_{s_k}	and snow, respectively
N_{CCN_k}	specific number of CCN in category k
N_{f_k}	specific number of frozen drops in category k
$N_{act\ ice}$	specific number of activated ice nuclei
$\bar{N}_{act}$	specific number of activated drops at a certain supersaturation
N_0, N_{0_k}	empirical parameters
N_{Sc}, N_{Re}, N_{Pr}	Schmidt, Reynolds, and Prandtl numbers, respectively
p_k	ratio between the mass in category $k + 1$ and the mass in k
$P_{w/i}$, $R_{w/i}$	functions of P, T and the distribution functions of the particles, used in the diffusional growth process

$P(x : m, y)$ distribution function of drop fragments x resulting from a collision between m and y
q_v specific humidity
$q_{s,w}$; $q_{s,i}$ saturation specific humidity with respect to water and ice, respectively
r, z radial and vertical coordinates, respectively
r_x radius of particle of type x (drops, ice crystal, snow, or graupel)
$\bar{r}$ average radius
$\bar{r}_{\max}$, $\bar{S}$ maximum average radius and average supersaturation, respectively, used for establishing the average radius of the newborn drops
R universal gas constant
R_v specific gas constant for water vapor
S_w, S_i supersaturation with respect to water and ice, respectively (in %)
T air temperature
t time
t_{ch} characteristic time of the simulation
u, w radial and vertical velocity components, respectively
v_x, v_{x_k} terminal velocity for particles of type x and in category k, respectively
x represents one of the ice species (ice crystals, graupel, or snow)
y represents one of the cloud species (drops, ice crystals, graupel, or snow)
α, β, γ parameters
$(\delta\varphi/\delta t)_{xxx}$ rate of change of parameter φ due to microphysical process xxx
ΔS_w, ΔS_i specific humidity surplus with respect to water and to ice, respectively [see definitions in Eqs. (B1) and (B2)]
Δt time step
ΔT subfreezing temperature
η kinematic viscosity
ρ_0 density of the unperturbed atmosphere
$\rho_a(z)$ density of air at height z
τ, τ_w, τ_i functions used in the diffusional growth and melting processes
$\bar{\xi}_{1/3}$ nondimensional parameters

APPENDIX B

Simultaneous Growth of Drops and Ice by Diffusion

The specific humidity surpluses with respect to water and to ice are defined as

$$\Delta S_w(t) = q_v - q_{s,w} \tag{B1}$$

and

$$\Delta S_i(t) = q_v - q_{s,i}, \tag{B2}$$

respectively.

The rate of change of the specific vapor and the temperature due to diffusional growth is given by

$$\frac{\partial q_v}{\partial t} = -\left[\left(\frac{\partial M_w}{\partial t}\right) + \sum_{x=i,g,s}\left(\frac{\partial M_x}{\partial t}\right)\right] \tag{B3}$$

and

$$\frac{\partial T}{\partial t} = \frac{L}{c_p}\left(\frac{\partial M_w}{\partial t}\right) + \frac{L_{vi}}{c_p}\sum_{x=i,g,s}\left(\frac{\partial M_x}{\partial t}\right). \tag{B4}$$

Taking the time derivative of Eq. (B1) and inserting Eqs. (B2) and (B3), we get an expression for the rate of change of the specific humidity surplus:

$$\begin{aligned}\frac{\partial \Delta S_w}{\partial t} &= \frac{\partial q_v}{\partial t} - \frac{\partial q_{s,w}}{\partial t} = \frac{\partial q_v}{\partial t} - \frac{\partial q_{s,w}}{\partial T}\frac{\partial T}{\partial t} \\ &= -\left(\frac{\partial M_w}{\partial t}\right) - \sum_{x=i,g,s}\left(\frac{\partial M_x}{\partial t}\right) - \frac{\partial q_{s,w}}{\partial T} \\ &\quad \times \left[\frac{L}{c_p}\left(\frac{\partial M_w}{\partial t}\right) + \frac{L_{vi}}{c_p}\sum_{x=i,g,s}\left(\frac{\partial M_x}{\partial t}\right)\right] \\ &= -\left[1 + \frac{L}{c_p}\left(\frac{\partial q_{s,w}}{\partial T}\right)\right]\left(\frac{\partial M_w}{\partial t}\right) \\ &\quad - \left[1 + \frac{L_{vi}}{c_p}\left(\frac{\partial q_{s,w}}{\partial T}\right)\right]\sum_{x=i,g,s}\left(\frac{\partial M_x}{\partial t}\right).\end{aligned} \tag{B5}$$

Similarly, for ice,

$$\begin{aligned}\frac{\partial \Delta S_i}{\partial t} &= -\left[1 + \frac{L}{c_p}\left(\frac{\partial q_{s,i}}{\partial T}\right)\right]\left(\frac{\partial M_w}{\partial t}\right) \\ &\quad - \left[1 + \frac{L_{vi}}{c_p}\left(\frac{\partial q_{s,i}}{\partial T}\right)\right]\sum_{x=i,g,s}\left(\frac{\partial M_x}{\partial t}\right).\end{aligned} \tag{B6}$$

In order to get an expression for the rate of change of the mass $(\partial M/\partial t)$, we integrate Eq. (21) over the entire spectrum:

$$\left(\frac{\partial M_y}{\partial t}\right)_{\text{cond/evap,depos/sublim}} = \int_0^\infty n_y(m,t)\left(\frac{dm}{dt}\right)_{\text{cond/evap,depos/sublim}} dm$$

$$= C_{w/x}(P,T)\Delta S_{w/i}\int_0^\infty m^{1/3} n_y(m,t)dm. \quad \text{(B7)}$$

Replacing this last expression in Eqs. (B5) and (B6), we get a set of two partially coupled differential equations of the form

$$\frac{\partial \Delta S_w(t)}{\partial t} + R_w \Delta S_w(t) + P_i \Delta S_i(t) = 0 \quad \text{(B8)}$$

and

$$\frac{\partial \Delta S_i(t)}{\partial t} + R_i \Delta S_i(t) + P_w \Delta S_w(t) = 0. \quad \text{(B9)}$$

The different functions are defined as follows:

$$R_w = A_w(P,T)C_w(P,T)\int_0^\infty m^{1/3} n_w(m,t)dm, \quad \text{(B10)}$$

$$R_i = B_i(P,T)\sum_{x=i,g,s} C_x(P,T)\int_0^\infty m^{1/3} n_x(m,t)dm, \quad \text{(B11)}$$

$$P_w = A_i(P,T)C_w(P,T)\int_0^\infty m^{1/3} n_w(m,t)dm, \quad \text{(B12)}$$

$$P_i = B_w(P,T)\sum_{x=i,g,s} C_x(P,T)\int_0^\infty m^{1/3} n_x(m,t)dm, \quad \text{(B13)}$$

where

$$A_w[P(t),T(t)] = 1 + \frac{L}{c_p}\frac{dq_{s,w}}{dT}, \quad \text{(B14)}$$

$$A_i[P(t),T(t)] = 1 + \frac{L}{c_p}\frac{dq_{s,i}}{dT}, \quad \text{(B15)}$$

$$B_w[P(t),T(t)] = 1 + \frac{L_{vi}}{c_p}\frac{dq_{s,w}}{dT}, \quad \text{(B16)}$$

$$B_i[P(t),T(t)] = 1 + \frac{L_{vi}}{c_p}\frac{dq_{s,i}}{dT}. \quad \text{(B17)}$$

The integral $\int m^{1/3} n(m,t)dm$ is approximated over the discrete spectrum according to Tzivion et al. (1989):

$$\int_0^\infty m^{1/3} n(m,t)dm \Rightarrow \bar{\xi}_{1/3}\sum_{k=1}^{J} \bar{m}_k^{1/3} N_k(t), \quad \text{(B18)}$$

where $\bar{\xi}_{1/3}$ is a nondimensional parameter very close to 1.

From Eq. (B8) and (B9) we can write

$$\frac{\partial^2 \Delta S_w(t)}{\partial t^2} + (R_w + R_i)\frac{\partial \Delta S_w(t)}{\partial t} + (R_w R_i - P_i P_w)\Delta S_w(t) = 0, \quad \text{(B19)}$$

with a solution

$$\Delta S_w(t) = c_1 e^{-m_1 t} + c_2 e^{-m_2 t}, \quad \text{(B20)}$$

where

$$m_{1,2} = \{-(R_w + R_i) \pm [(R_w + R_i)^2 - 4(R_w R_i - P_w P_i)]^{1/2}\}/2. \quad \text{(B21)}$$

Putting Eq. (B20) into (B9), we get an equation for ΔS_i:

$$\Delta S_i(t) = c_1\delta_1 e^{-m_1 t} + c_2\delta_2 e^{-m_2}, \quad \text{(B22)}$$

where

$$\delta_1 = \left(\frac{m_1 - R_w}{P_i}\right), \quad \text{and} \quad \delta_2 = \left(\frac{m_2 - R_w}{P_i}\right). \quad \text{(B23)}$$

The coefficients c_1 and c_2 can be found by setting initial conditions at $t = t_0$:

$$c_1 = \frac{\Delta S_w(t_0)\delta_2 - \Delta S_i(t_0)}{\delta_2 - \delta_1} \quad \text{and}$$

$$c_2 = \frac{\Delta S_i(t_0) - \Delta S_w(t_0)\delta_1}{\delta_2 - \delta_1}. \quad \text{(B24)}$$

We solve the equation for one time step ($t \rightarrow t + \Delta t$) and we assume that during that time $R_{w,i}$ and $P_{w,i}$ remain constant. Using Eqs. (B10)–(B16), the discriminant in Eq. (B21) can be written

$$(R_w R_i - P_w P_i) \approx 0. \quad \text{(B25)}$$

Therefore,

$$m_1 = 0, \quad \text{and} \quad m_2 = -(R_w + R_i). \quad \text{(B26)}$$

Finally, the solution for $\Delta S_w(t + \Delta t)$ is

$$\Delta S_w(t + \Delta t) = \Delta S_w(t) - \frac{[R_w \Delta S_w(t) + P_i \Delta S_i(t)]}{(R_w + R_i)} \times [1 - \exp^{-(R_w + R_i)\Delta t}] \quad \text{(B27)}$$

and similarly for $\Delta S_i(t + \Delta t)$ is

$$\Delta S_i(t + \Delta t) = \Delta S_i(t) - \frac{[R_i \Delta S_i(t) + P_w \Delta S_w(t)]}{(R_w + R_i)} \times [1 - \exp^{-(R_w + R_i)\Delta t}]. \quad \text{(B28)}$$

When ΔS_w or ΔS_i change sign during one time step, as explained in section 2, we find the appropriate Δt^*

by solving for t when Eqs. (B27) and (B28) are equal to zero. Thus, we get

$$\Delta t_w^* = \frac{1}{(R_w + R_i)} \ln\left[\frac{1 + (R_w/P_i)(\Delta S_w/\Delta S_i)}{1 - (R_i/P_i)(\Delta S_w/\Delta S_i)}\right] \quad \text{(B29)}$$

and

$$\Delta t_i^* = \frac{1}{(R_w + R_i)} \ln\left[\frac{1 + (R_i/P_w)(\Delta S_i/\Delta S_w)}{1 - (R_w/P_w)(\Delta S_i/\Delta S_w)}\right]. \quad \text{(B30)}$$

APPENDIX C

The Stochastic Collection Equation for Two or More Interacting Species

A set of four coupled stochastic equations can be formulated for the four distribution functions of the different species. The gain and loss terms are annotated according to the result of the specific interaction as described in Table 1:

$$\frac{\partial n_y(m, z, r, t)}{\partial t} = \sum_{y_1, y_2 = w,i,g,s} \delta_{y_1,y_2} \int_0^{m/2} n_{y_1}(m - x, z, r, t) n_{y_2}(x, z, r, t) C_{y_1,y_2}(m - x, x) dx - n_y(m, z, r, t)$$
$$\times \sum_{y^* = w,i,gs} \int_0^{\infty} n_{y^*}(x, z, r, t) C_{y,y^*}(m, x) dx + \delta_{yw}\left[\int_0^{\infty} n_w(x, z, r, t) dx \int_0^{x} n_w(y, z, r, t) B(x, y)\right.$$
$$\left. \times P(m; x, y) dy - n_w(m, z, r, t) \int_0^{\infty} \frac{n_w(y, z, r, t) B(m, y)}{m + y} dy \int_0^{m+y} x P(x; m, y) dx\right], \quad \text{(C1)}$$

where y is for w, i, g, or s. The Kroenecker delta is used to select the interactions that produce a gain term for the species y. The first term on the right side of Eq. (C1) is for the gain interactions in the number of particles of mass m by the coalescence of all masses x and $m - x$. The second one is for the loss interactions between species y with itself and with the other species. The two last terms are according to Feingold et al.'s (1988) formulation for the collisional breakup of water drops. The third term is the gain in the number of drops of mass m created by the collisional breakup of all masses x and y ($x + y = m$), and the last term is the number of drops of mass m lost through collision and subsequent breakup of drops of mass m and y.

The collection kernel between particles of type a and b is $C_{a,b}(x, y)$, and $B(x, y)$ is the breakup kernel. Both are assumed to be independent of (z, r) and are defined by

$$C_{a,b}(x, y) = K_{a,b}(x, y) E_{a,b}(x, y)$$
$$B(x, y) = K_{w,w}(x, y)[1 - E_{w,w}(x, y)]. \quad \text{(C2)}$$

Further, $K_{a,b}(x, y)$ is the gravitational geometric collection kernel for particles of type a and b with masses x and y, respectively, and $E_{a,b}(x, y)$ is the collection (collision + coalescence) efficiency for particles a and b with masses x and y, respectively. For drops, we assume that collection and breakup are mutually exclusive. Cases of bounce are not considered since they do not change the spectrum. The distribution function of drop fragments of mass x resulting from a collision between m and y is $P(x; m, y)$.

As explained in section 2, the equations for the moments of the distribution function are divided into gain and loss terms according to the different interactions between the particles. As an example, we consider collision–coalescence between drops and graupel. Since all the interactions between drops and graupel produce graupel, the number and mass concentrations in category k for the drops is schematically written as

$$N_{n_k} = GN_{(n,n)_k} - LN_{(n,n)_k} - LN_{(n,g)_k} \quad \text{(C3)}$$

$$M_{n_k} = GM_{(n,n)_k} - LM_{(n,n)_k} - LM_{(n,g)_k} \quad \text{(C4)}$$

and for the graupel as

$$N_{g_k} = GN_{(g,g)_k} + GN_{(g>n)_k} + GN_{(n>g)_k} - LN_{(g,g)_k} - LN_{(g,n)_k} \quad \text{(C5)}$$

$$M_{g_k} = GM_{(g,g)_k} + GM_{(g>n)_k} + GM_{(n>g)_k} - LM_{(g,g)_k} - LM_{(g,n)_k}. \quad \text{(C6)}$$

The "GN" and "GM" terms represent gain terms for the number and mass concentrations, respectively, and the "LN" and "LM" are the loss terms. Each of these terms describes a certain type of interaction that can be physically explained. In the following, an explanation for each of these terms is given. Here, n_k represents the distribution function for the drops at category k, and g_k is for the distribution function of graupel at category k.

$$GN_{(n,n)_k} = \sum_{i=1}^{k-2} \int_{x_i}^{x_{i+1}} n_i(x,t)dx \int_{m_k-x}^{m_k} n_{k-1}(m,t)C_{k-1,i}^{n,n} \times (m,x)dm + \frac{1}{2}\int_{m_{k-1}}^{m_k} n_{k-1}(x,t)dx \times \int_{m_{k-1}}^{m_k} n_{k-1}(m,t)C_{k-1,k-1}^{n,n}(m,x)dm. \quad \text{(C7)}$$

This is the gain term for the number concentration of the drops due to interactions between the drops themselves. The first term is for the drops that enter k as a result of interactions between the tail of $k-1$ and lower categories. The second term is for drops in $k-1$ that coalesce and enter k; the factor $1/2$ is because for two drops that coalesce in $k-1$, one enters k.

$$LN_{(n,n)_k} = \sum_{i=1}^{k-1} \int_{x_i}^{x_{i+1}} n_i(x,t)dx \int_{m_{k+1}-x}^{m_{k+1}} n_k(m,t)C_{k,i}^{n,n} \times (m,x)dm + \sum_{i=k}^{I} \int_{x_i}^{x_{i+1}} n_i(x,t)dx \times \int_{m_k}^{m_{k+1}} n_k(m,t)C_{i,k}^{n,n}(x,m)dm. \quad \text{(C8)}$$

This is the loss term for the number concentration of the drops due to interactions between the drops themselves. The first term is for the drops that leave k as a result of interactions between the tail of k and lower categories. The second term is for drops that leave k due to coalescence with drops at higher categories.

$$LN_{(n,g)_k} = \sum_{i=1}^{I} \int_{x_i}^{x_{i+1}} g_i(x,t)dx \times \int_{m_k}^{m_{k+1}} n_k(m,t)C_{i,k}^{n,g}(x,m)dm. \quad \text{(C9)}$$

This is the loss term for the number concentration of the drops due to interactions between drops and graupel. It represents the drops in k that coalesce with graupel and leave the category, since all the interactions between drops and graupel produce graupel.

$$GM_{(n,n)_k} = \sum_{i=1}^{k-2} \int_{x_i}^{x_{i+1}} n_i(x,t)dx \int_{m_k-x}^{m_k} (m+x)n_{k-1} \times (m,t)\, C_{k-1,i}^{n,n}(m,x)dm + \int_{m_{k-1}}^{m_k} n_{k-1}(x,t)dx \times \int_{m_{k-1}}^{m_k} mn_{k-1}(m,t)C_{k-1,k-1}^{n,n}(m,x)dm + \sum_{i=1}^{k-1} \int_{x_i}^{x_{i+1}} xn_i(x,t)dx \times \int_{m_k}^{m_{k+1}-x} n_k(m,t)C_{k,i}^{n,n}(m,x)dm. \quad \text{(C10)}$$

This is the gain term for the mass concentration of the drops, and the first two terms are analogous to Eq. (C7). The third term is for drops in the beginning of k that interact with smaller drops and add mass x to the category.

$$LM_{(n,n)_k} = \sum_{i=1}^{k-1} \int_{x_i}^{x_{i+1}} n_i(x,t)dx \times \int_{m_{k+1}-x}^{m_{k+1}} mn_k(m,t)C_{k,i}^{n,n}(m,x)dm + \sum_{i=k}^{I} \int_{x_i}^{x_{i+1}} n_i(x,t)dx \times \int_{m_k}^{m_{k+1}} mn_k(m,t)C_{i,k}^{n,n}(x,m)dm. \quad \text{(C11)}$$

This equation is similar to Eq. (C8) except that it represents the loss term of the mass concentration of drops due to their interaction with other drops.

$$LM_{(n,g)_k} = \sum_{i=1}^{I} \int_{x_i}^{x_{i+1}} g_i(x,t)dx \times \int_{m_k}^{m_{k+1}} mn_k(m,t)C_{i,k}^{n,g}(x,m)dm. \quad \text{(C12)}$$

This is the loss term for the mass concentration of the drops due to interactions between drops and graupel and it is analogous to Eq. (C9).

$$GN_{(g>n)_k} = \sum_{i=1}^{k-2} \int_{x_i}^{x_{i+1}} n_i(x,t)dx \times \int_{m_k-x}^{m_k} g_{k-1}(m,t)C_{k-1,i}^{g,n}(m,x)dm + \frac{1}{2}\int_{m_{k-1}}^{m_k} n_{k-1}(x,t)dx \times \int_{m_{k-1}}^{m_k} g_{k-1}(m,t)C_{k-1,k-1}^{g,n}(m,x)dm. \quad \text{(C13)}$$

This is the gain term for the number concentration of graupel due to interactions between graupel and drops, when the graupel are bigger than the drops. The first term is for interactions between graupel in the tail of $k-1$ and drops in lower categories. The second term is for graupel in $k-1$ that coalesce with drops in $k-1$ and enter k; the factor $1/2$ is because of symmetry.

$$LN_{(g,n)_k} = \sum_{i=1}^{k-1} \int_{x_i}^{x_{i+1}} n_i(x,t)dx \times \int_{m_{k+1}-x}^{m_{k+1}} g_k(m,t)C_{k,i}^{g,n}(m,x)dm$$

$$+\sum_{i=k}^{I}\int_{x_i}^{x_{i+1}} n_i(x,t)dx \times \int_{m_k}^{m_{k+1}} g_k(m,t)C_{i,k}^{g,n}(x,m)dm. \quad \text{(C14)}$$

This is the loss term for the number concentration of the graupel due to interactions between graupel and drops. The first term is for graupel that leave k as a result of interactions between the tail of k and lower categories of drops. The second term is for graupel in k that coalesce with drops from higher categories.

$$GN_{(n>g)_k} = \sum_{i=1}^{k-2}\int_{x_i}^{x_{i+1}} g_i(x,t)dx \times \int_{m_k-x}^{m_k} n_{k-1}(m,t)C_{k-1,i}^{n,g}(m,x)dm + \sum_{i=1}^{k-1}\int_{x_i}^{x_{i+1}} g_i(x,t)dx \times \int_{m_k}^{m_k+1-x} n_k(m,t)C_{k,i}^{n,g}(m,x)dm + \frac{1}{2}\int_{m_{k-1}}^{m_k} g_{k-1}(x,t)dx \times \int_{m_{k-1}}^{m_k} n_{k-1}(m,t)C_{k-1,k-1}^{n,g}(m,x)dm. \quad \text{(C15)}$$

This is the gain term for the number concentration of graupel due to interactions between drops and graupel when the drops are bigger than the graupel. The first term is for interactions between drops in the tail of $k-1$ and graupel in lower categories. The second term is for drops at the beginning of k that interact with graupel at lower categories and enter k of the graupel. The third term is for drops in $k-1$ that coalesce with graupel in $k-1$ and enter k; the factor $1/2$ is because of symmetry.

$$GM_{(g>n)_k} = \sum_{i=1}^{k-2}\int_{x_i}^{x_{i+1}} n_i(x,t)dx \times \int_{m_k-x}^{m_k} (m+x)g_{k-1}(m,t)C_{k-1,i}^{g,n}(m,x)dm + \int_{m_{k-1}}^{m_k} n_{k-1}(x,t)dx \times \int_{m_{k-1}}^{m_k} mg_{k-1}(m,t)C_{k-1,k-1}^{g,n}(m,x)dm + \sum_{i=1}^{k-1}\int_{x_i}^{x_{i+1}} xn_i(x,t)dx \times \int_{m_k}^{m_{k+1}-x} g_k(m,t)C_{k,i}^{g,n}(m,x)dm. \quad \text{(C16)}$$

This is the gain term for the mass concentration of the graupel due to interactions between graupel and drops, in the case of the graupel is bigger than the drops. The first term is for mass $(m+x)$ that enters k as a result of interactions between the tail of the graupel $k-1$ (with mass m) and lower categories of drops (with mass x). The second term is for graupel in $k-1$ and drops in $k-1$ that coalesce and enter k, adding mass m. The third term is for graupel in the beginning of k that interact with drops from lower categories and add mass x.

$$LM_{(g,n)_k} = \sum_{i=1}^{k-1}\int_{x_i}^{x_{i+1}} n_i(x,t)dx \times \int_{m_{k+1}-x}^{m_{k+1}} mg_k(m,t)C_{k,i}^{g,n}(m,x)dm + \sum_{i=k}^{I}\int_{x_i}^{x_{i+1}} n_i(x,t)dx \times \int_{m_k}^{m_{k+1}} mg_k(m,t)C_{i,k}^{g,n}(x,m)dm. \quad \text{(C17)}$$

This is the loss term for the mass concentration of the graupel due to interactions between graupel and drops and it is analogous to Eq. (C14).

$$GM_{(n>g)_k} = \sum_{i=1}^{k-2}\int_{x_i}^{x_{i+1}} g_i(x,t)dx \times \int_{m_k-x}^{m_k} (m+x)n_{k-1}(m,t)C_{k-1,i}^{n,g}(m,x)dm + \int_{m_{k-1}}^{m_k} g_{k-1}(x,t)dx \times \int_{m_{k-1}}^{m_k} mn_{k-1}(m,t)C_{k-1,k-1}^{n,g}(m,x)dm + \sum_{i=1}^{k-1}\int_{x_i}^{x_{i+1}} (m+x)g_i(x,t)dx \times \int_{m_k}^{m_{k+1}-x} n_k(m,t)C_{k,i}^{n,g}(m,x)dm. \quad \text{(C18)}$$

This equation is similar to (C15) except it represents the gain term for the mass concentration of graupel particles due to their interactions with larger drops:

Equations (C7), (C8), (C10), and (C11) can be used to calculate the terms $GN_{(g,g)_k}$, $LN_{(g,g)_k}$, $GM_{(g,g)_k}$, and $LM_{(g,g)_k}$, respectively, in Eq. (C5) by replacing all the n with g (subscripts, superscripts, and otherwise).

In a similar way, we formulate the expressions for the interactions with the other species (ice crystals and snow).

REFERENCES

Alheit, R. R., A. I. Flossmann, and H. R. Pruppacher, 1990: A theoretical study of the wet removal of atmospheric pollutants. Part IV: The uptake and redistribution of aerosol particles through nucleation and impaction scavenging by growing cloud drops and ice particles. *J. Atmos. Sci.*, **47**, 870–887.

Auer, A. H., and D. L. Veal, 1970: The dimension of ice crystals in natural clouds. *J. Atmos. Sci.*, **27**, 919–926.

Beard, K. V., 1976: Terminal velocity adjustment for cloud and precipitation. *J. Atmos. Sci.*, **33**, 851–864.

Bigg, E. K., 1953: The formation of atmospheric ice crystals by the freezing of droplets. *Quart. J. Roy. Meteor. Soc.*, **79**, 510–519.

Bleck, R., 1970: A fast approximative method for integrating the stochastic coalescence equation. *J. Geophys. Res.*, **75**, 5165–5171.

Böhm, H. P., 1989: A general equation for the terminal fall speed of solid hydrometeors. *J. Atmos. Sci.*, **46**, 2419–2427.

Bryan, K., 1966: A scheme for numerical integration of the equation of motion on an irregular grid free of nonlinear instability. *Mon. Wea. Rev.*, **94**, 39–41.

Chen, J. P., 1992: Numerical simulation of the redistribution of atmospheric trace chemicals through cloud processes. Ph.D. thesis, The Pennsylvania State University, 342 pp.

Clark, T. L., 1974: On modelling nucleation and condensation theory in Eulerian spatial domain. *J. Atmos. Sci.*, **31**, 2099–2117.

Cotton, W. R., 1972: Numerical simulation of precipitation development in supercooled cumuli—Part II. *Mon. Wea. Rev.*, **100**, 764–784.

——, and R. A. Anthes, 1989: *Storm and Cloud Dynamics.* International Geophysics Series, Vol. 44, Academic Press, 883 pp.

Danielsen, E. F., R. Bleck, and D. A. Morris, 1972: Hail growth by stochastic collection in a cumulus model. *J. Atmos. Sci.*, **29**, 135–155.

Feingold, G., S. Tzivion, and Z. Levin, 1988: The evolution of raindrop spectra. Part I: Stochastic collection and breakup. *J. Atmos. Sci.*, **45**, 3387–3399.

——, Z. Levin, and S. Tzivion, 1991: The evolution of raindrop spectra. Part III: Downdraft generation in an axisymmetrical rainshaft model. *J. Atmos. Sci.*, **48**, 315–330.

Flossmann, A. I., 1991: The scavenging of two different types of marine aerosol particles calculated using a two-dimensional detailed cloud model. *Tellus*, **43B**, 301–321.

——, W. D. Hall, and H. R. Pruppacher, 1985: A theoretical study of the wet removal of atmospheric pollutants. Part I: The redistribution of aerosol particles captured through nucleation and impaction scavenging by growing cloud drops. *J. Atmos. Sci.*, **42**, 582–606.

Hall, W. D., 1980: A detailed microphysical model within a two-dimensional dynamic framework: Model description and preliminary results. *J. Atmos. Sci.*, **37**, 2486–2507.

Hallet, J., and S. C. Mossop, 1974: Production of secondary ice crystals during the riming process. *Nature*, **249**, 26–28.

Khvorostyanov, V. I., A. P. Khain, and E. A. Kogteva, 1989: Two-dimensional nonstationary microphysical model of a three-phase convective cloud and evaluation of the effects of seeding by a crystallizing agent. *Sov. Meteor. Hydrol.*, **5**, 33–45.

Kogan, Y. L., 1991: The simulation of a convective cloud in a 3-D model with explicit microphysics. Part I: Model description and sensitivity experiments. *J. Atmos. Sci.*, **48**, 1160–1189.

Lew, J. K., D. E. Kingsmill, and D. C. Montague, 1985: A theoretical study of the collision efficiency of small planar ice crystals colliding with large supercooled water drops. *J. Atmos. Sci.*, **42**, 857–862.

Long, A. B., 1974: Solutions to the droplet coalescence equation for polynomial kernels. *J. Atmos. Sci.*, **31**, 1040–1057.

Low, T. B., and R. List, 1982a: Collision, coalescence and breakup of raindrops. Part I: Experimentally established coalescence efficiencies and fragments size distribution in breakup. *J. Atmos. Sci.*, **39**, 1591–1606.

——, and ——, 1982b: Collision, coalescence and breakup of raindrops. Part II: Parameterization of fragment size distributions in breakup. *J. Atmos. Sci.*, **39**, 1607–1618.

Martin, J. J., P. K. Wang, and H. R. Pruppacher, 1982: A numerical study of the effect of electric charges on the efficiency with which planar ice crystals collect supercooled cloud drops. *J. Atmos. Sci.*, **39**, 2462–2469.

Meyers, M. P., P. J. DeMott, and W. R. Cotton, 1992: New primary ice-nucleation parameterizations in an explicit cloud model. *J. Appl. Meteor.*, **31**, 708–721.

Monin, A. C., and A. M. Yaglom, 1967: *Statistical Hydromechanics.* Part 2. Izdatelstvo Nauka, 720 pp.

Nelson, L., 1979: Observations and numerical simulations of precipitation in natural and seeded convective clouds. Ph.D. thesis, University of Chicago, 157 pp. [Available from Cloud Physics Laboratory, University of Chicago, Chicago IL 60637.]

Ochs, H. T., R. R. Czys, and K. V. Beard, 1986: Laboratory measurements of coalescence efficiencies for small precipitating drops. *J. Atmos. Sci.*, **43**, 225–232.

Ogura, Y., and T. Takahashi, 1973: The development of warm rain in a cumulus cloud. *J. Atmos. Sci.*, **30**, 262–277.

Orville, H. D., and F. J. Kopp, 1977: Numerical simulations of the history of a hailstorm. *J. Atmos. Sci.*, **34**, 1596–1618.

Pruppacher, H. R., and J. D. Klett, 1978: *Microphysics of Clouds and Precipitation.* D. Reidel, 714 pp.

Rasmussen, R. M., and A. J. Heymsfield, 1985: A generalized form for impact velocities used to determine graupel accretional densities. *J. Atmos. Sci.*, **42**, 2275–2279.

——, and ——, 1987: Melting and shedding of graupel and hail. Part I: Model physics. *J. Atmos. Sci.*, **44**, 2754–2763.

Reisin, T., S. Tzivion, Z. Levin, and G. Feingold, 1988: Numerical simulation of an Hawaiian convective cloud with a high resolution axisymmetric model. *Proc. Second WMO Int. Cloud Modelling Workshop*, Toulouse, France, World Meteorological Organization, 231–235.

Scott, B. C., and P. V. Hobbs, 1977: A theoretical study of the evolution of mixed-phase cumulus clouds. *J. Atmos. Sci.*, **34**, 812–826.

Smolarkiewicz, P. K., 1983: A simple positive definite advection scheme with small implicit diffusion. *Mon. Wea. Rev.*, **111**, 479–486.

Soong, S., 1974: Numerical simulation of warm rain development in an axisymmetric cloud model. *J. Atmos. Sci.*, **31**, 1262–1285.

Takahashi, T., 1976: Hail in an axisymmetric cloud model. *J. Atmos. Sci.*, **33**, 1579–1601.

Twomey, S., 1959: The nuclei of natural cloud formation: The supersaturation in natural clouds and the variation of cloud droplets concentrations. *Geofis. Pura Appl.*, **43**, 243–249.

Tzivion, S., 1980: A numerical solution of the kinetic coalescence. *Eighth Int. Conf. on Cloud Physics*, Clermont-Ferrand, France, ICCP, 87–90.

——, Z. Levin, and A. Manes, 1984: Numerical simulation of the effects of stable region aloft on the development of thermal convection. *Proc. of the Ninth Int. Cloud Physics Conf.*, Tallin, USSR, ICCP, 537–540.

——, G. Feingold, and Z. Levin, 1987: An efficient numerical solution to the stochastic collection equation. *J. Atmos. Sci.*, **44,** 3139–3149.

——, ——, and ——, 1989: The evolution of raindrop spectra. Part II: Collisional collection/breakup and evaporation in a rainshaft. *J. Atmos. Sci.*, **46,** 3312–3327.

——, T. Reisin, and Z. Levin, 1994: Numerical simulation of hygroscopic seeding in a convective cloud. *J. Appl. Meteor.*, **33,** 252–267.

Tzur, I., and Z. Levin, 1981: Ions and precipitation charging in warm and cold clouds as simulated in one-dimensional time-dependent models. *J. Atmos. Sci.*, **38,** 2444–2461.

Young, K. C., 1974a: A numerical simulation of wintertime, orographic precipitation. Part I: Description of model microphysics and numerical techniques. *J. Atmos. Sci.*, **31,** 1735–1748.

——, 1974b: A numerical simulation of wintertime, orographic precipitation. Part II: Comparison of natural and AgI-seeded conditions. *J. Atmos. Sci.*, **31,** 1749–1767.

Walko, R. L., W. R. Cotton, M. P. Meyers, and J. L. Harrington, 1995: New RAMS cloud microphysics parameterization. Part I: The single-moment scheme. *Atmos. Res.*, **38,** 29–62.

Wang, C., and J. S. Chang, 1993: A three-dimensional numerical model of cloud dynamics, microphysics, and chemistry. 1. Concepts and formulation. *J. Geophys. Res.*, **98,** 14 827–14 844.